Title: Leaf venation network evolution across clades and scales

Author list:

1,2 Ilaine Silveira Matos, ilaine.matos@gmail.com
1 Bradley Vu, bradleydvu@berkeley.edu
1 Joseph Mann, jmann2@berkeley.edu
1 Emily Xie, emily.x@berkeley.edu
1 Srinivasan Madhavan, seenum@berkeley.edu
1 Satvik Sharma, satvik.sharma@berkeley.edu
1 Izzi Niewiadomski, iniewiadomski@berkeley.edu
1 Andrea Echevarria, andrea.de@berkeley.edu
1 Connor Tomaka, ctomakai@gmail.com
1 Sonoma Carlos, sonomacarlos@berkeley.edu
1 Monica Antonio, monica25antonio@berkeley.edu
1 Ashley Chu, chu00015@berkeley.edu
1 Meg Scudder, megfds@berkeley.edu
1 Nicole Yokota, nyokota@berkeley.edu
1,3 Hailey J. Park, haileypark@berkeley.edu
4 Natalie Vuong, nataliehtvuong@gmail.com
1 Mickey Boakye, mickeyboakye@berkeley.edu
5 Miguel A. Duarte, miguelduarte802@gmail.com
1 Caroline Pechuzal, pechuzal@gmail.com
6 Luiza Maria T. Aparecido, luiza.aparecido@biology.utah.edu
1 Mia B. Franco, miafranco@berkeley.edu
1 Ryan Jen Wong, ryanwong123@berkeley.edu
1 Jocelyn Liu, jocelyn.liu@berkeley.edu
5,7 Emily Guevara Heredia, emy_1996@hotmail.es
8 Brad Boyle, bboyle@arizona.edu
9 Martha Ryan, martryan@udel.edu
7 Rafael E. Cárdenas, recardenasm@yahoo.com
8 Brian J. Enquist, benquist@email.arizona.edu

10 Diane M. Erwin, dmerwin@berkeley.edu

11 Holly Forbes, hforbes@berkeley.edu11

12,13,14 Kyle Dexter, Kyle.Dexter@ed.ac.uk

15 Mark Fricker, mark.fricker@biology.ox.ac.uk

1 Benjamin W. Blonder, benjamin.blonder@berkeley.edu

Affiliations:

1 Department of Environmental Science, Policy, and Management, University of California Berkeley, Berkeley, CA 94720, USA

2 School of Biological Sciences, The University of Adelaide, Adelaide, SA 5005, Australia

3 Division of Infectious Diseases and Geographic Medicine, Department of Medicine, Stanford University, Stanford, CA, USA

4 Department of Biology, University of Waterloo, Waterloo, ON N2L 3G1, Canada

5 School of Life Sciences, Arizona State University, Tempe, AZ 85281, USA

6 School of Biological Sciences, The University of Utah, Salt Lake City, UT 84112, USA

7 Escuela de Ciencias Biológicas, Pontificia Universidad Católica del Ecuador, Apdo. 17-01-2184, Quito, Ecuador.

8 Department of Ecology & Evolutionary Biology, The University of Arizona, Tucson, AZ 85721, USA

9 Department of Plants & Soil Sciences, University of Delaware, Newark, DE 19716, USA

10 University of California Museum of Paleontology, Berkeley, CA 94720, USA

11 University of California Botanical Garden at Berkeley, CA 94720, USA

12 School of GeoSciences, University of Edinburgh, Edinburgh EH8 9YL, UK

13 Royal Botanic Garden Edinburgh, Edinburgh EH3 5NZ, UK

14 Department of Life Sciences, University of Turin, 10124 Torino TO, Italy

15 Department of Biology, University of Oxford, Oxford, OX1 3RB, UK

Corresponding Author:

* Ilaine Silveira Matos, ilaine.matos@gmail.com; +61 0410114683; 54 Mulford Hall, Berkeley, CA 94720, USA.

Abstract

Leaf venation architecture varies greatly amongst living and fossil plants. However, we still have a limited understanding of when, why, and in which clades new architectures arose, and how they impacted leaf functioning. Using data from 1,000 extant and extinct (fossil) plants we reconstructed ca. 400 Myr of venation evolution across clades and vein sizes. Overall, venation networks evolved from having fewer veins and less smooth loops, to having more veins and smoother loops, but these changes only occurred in small and medium vein sizes. The diversity of architectural designs increased biphasically, first peaking in the Paleozoic, then decreasing during the Cretaceous, then increasing again in the Cenozoic, when recent angiosperm lineages initiated a second and ongoing phase of diversification. Vein evolution was not associated with temperature and CO_2 fluctuations, but was associated with insect diversification. Our results highlight the complexity of the evolutionary trajectory and potential drivers of venation network architecture.

Keywords: leaf evolution, leaf form, megaphyll, plant macroevolution, plant phylogeny, vein architecture, vein density, venation networks.

Main text:

Introduction

The ca. 400 Myr of evolutionary history in vascular plant leaves has resulted in a diversity of venation network architectures in extant and extinct plants[1,2] (**Fig. 1**). Despite the importance of those architectural features to multiple leaf functions[3,4], many aspects of their evolution remain unresolved. This limits our capacity to assess the evolution of ecophysiology[1], reconstruct paleoclimate[5], and interpret plant-climate feedback across deep time[6].

Previous studies have reconstructed the evolution of individual venation traits, particularly minor vein density[1,7,8]. They revealed that an 8-fold increase in minor vein density in late angiosperm lineages led to a surge in photosynthetic capacity, with implications for terrestrial biogeochemistry and biodiversity[7–11] Minor vein density, however, is just one amongst many traits describing network architecture (**Fig. 2**). Many unknowns remain about when and in which

clades the evolution of novel trait-combinations originated[9,10], and whether the diversity of network architectures increased (by divergence) or decreased (by convergence or extinction) over time.

Venation traits vary systematically across vein sizes[3,4] and may also show different evolutionary lability, with traits in smaller veins thought to be more labile[3,11]. These differences suggest that venation traits could have followed distinct evolutionary trajectories across vein sizes[4], e.g., smaller veins (e.g., minor veins) evolving traits to optimize flow efficiency, and larger veins (e.g., major veins) developing features for mechanical strength[12]. Alternatively, complex architectures sometimes consist of highly integrated traits[13], such that a coordinated evolutionary response could exist across vein sizes (small, medium, large), vein orders (minor x major) and/or traits. Such hypotheses about independent versus coordinated venation evolution still remain largely untested, as previous studies have focused on a few venation traits, typically on subregions of leaves, and have included fossil taxa with limited temporal coverage[1,7,8].

The biotic and abiotic drivers of venation trait evolution are also uncertain. A decline in atmospheric CO_2 concentration during the Cretaceous is oftentimes linked to the evolution of networks with high minor vein density[6,10]. Much less is known about which environmental conditions caused changes in other venation features, e.g., in the density of larger veins, or the degree of looping in the network architecture. Simulations suggest that, in response to frequent damage[14], networks develop loops to bypass damaged areas. Therefore, the evolution of looping networks or of non-minor veins architectural features could be linked to increased damage pressure from herbivore evolution[15] or to fluctuations in climate, but these hypotheses have not yet been formally tested.

Here, we assembled venation networks for 1,000 extant (N=880) and extinct (N=120) plant taxa (**Fig.1**, **Supplementary Fig. 1**). Cleared leaf images or compression fossils representing whole (extant) or partial (extinct) leaves were traced and segmented, enabling extraction of multiple venation traits[3] (**Fig. 2**). By applying novel phylogenetic comparative methods[16], we were able to answer the following questions: (1) How did venation traits evolve across vein sizes (i.e., small, medium, large veins) and major clades? (2) How did the occupancy of morphospace change over

time? (3) How are each of climate and herbivory proxies correlated to leaf venation traits over time?

Results

Evolution of venation traits across clades and vein sizes.

Using phylogenetic ridge regressions incorporating internal node constraints derived from fossils[14], we inferred the evolutionary trajectories of venation networks across major plant clades and vein sizes (**Fig.3-4; Supplementary Data 1**). Considering all vascular plants, leaf venation networks evolved from initially having fewer veins and less smooth loops (lower *VD* and *CR* at small and medium veins), to more complex networks with more veins (higher VD_{small} and VD_{medium}), smoother loops (higher CR_{small} and CR_{medium}), and fewer loops (higher MST_{small} and MST_{medium}; **Fig.3**). Note that the decrease in MST_{small} over time does not suggest that leaves evolved towards completely non-reticulate networks (as MST_{small} did not evolve to 1, which would indicate fully branched networks). Instead, the trend in MST_{small} suggests the evolution of networks that still have loops, but might also have a larger proportion of internal free-ending veins. Supporting this idea, we further calculated the density of free-ending veins (FEV) for our investigated species (see **Supplementary Note 1**), and found a significant temporal trend of increased free-ending vein density over time for all vascular plants pooled together.

Significant evolutionary trends were only observed at small and medium vein sizes, while the architecture of larger veins has not shifted directionally over the ca. 400 Myr of vascular plant evolution. Even though we found small and significant differences in evolutionary rates of venation traits across vein sizes (**Extended Data Fig. 1**), there was no evidence of slower trait evolution in larger veins for any of the traits evaluated. That is, evolutionary rates of venation traits in larger veins did not differ, or were higher (not lower) than in small/medium veins. Overall, our sensitivity analysis (**Supplementary Data 2**) indicated that these observed patterns were robust to subsampling and uncertainties associated with phylogenetic placement and age of fossils.

Importantly, in some samples, we were unable to segment very small veins (veins with width < 10 □m). Therefore, FEV density calculated here might not have captured all free ending veinlets

in all species, nor were the FEVs in this study defined based on terms of their developmental features. Arguably, even if minor veins are missing in some samples, our estimates of vein traits for larger vein scales are still relevant - particularly because their evolution has been largely unexplored in previous studies. Additionally, our vein size classification into small, medium, and large veins (see **Online Methods** for more details) does not necessarily coincide with the traditional classification of primary (major), secondary, and tertiary (minor) veins, nor considers vein tapering (see **Extended Data Fig. 2)**.

Despite those general patterns, when we looked at the evolutionary trends within each major plant clade, we found that clades sometimes followed distinct trajectories both in terms of magnitude and direction of trait change over time (**Fig. 4**; **Extended Data Fig. 2**). For example, while gymnosperms, monocots, and rosids showed a clear temporal increase in vein density (**Extended Data Fig. 3a-b**), no significant trend in *VD* was observed in other plant clades (**Supplementary Data 3**). Similarly, networks evolved fewer loops at small and/or medium veins in most clades, except in monocots and rosids which showed the opposite pattern of evolution (**Extended Data Fig. 3d-e**). Together, these results show that directional evolution of venation traits occurred for some but not all components of network architecture, and only for certain clades and vein sizes.

Changes in morphospace occupancy over time.

Using a principal component analysis with the reconstructed venation trait values (**Fig. 5a**), we calculated two complementary metrics of morphospace disparity that described the position (median centroids) and the extent (sum variances) of space occupied by each clade. We then found that ferns, gymnosperms, and monocots explored a higher diversity of architectures than any eudicot clade (**Fig. 5b-c**).

When we conducted a disparity-through-time analysis at ca.10 Myrs time-slices (**Supplementary Data 4**), we found that the disparity in architectures showed a biphasic increase (**Fig. 5d**) and followed a model of evolution constrained towards an optimum (i.e., Ornstein-Uhlenbeck model; see **Supplementary Data 5**). That is, vascular plants explored a greater diversity of architectures midway through their evolutionary history, with a peak in disparity in the Mesozoic period (ca. 200-150 Mya), when ferns and gymnosperms dominated the terrestrial

flora. Then, with the advent of angiosperms during the Cretaceous (ca. 125-80 Mya), the disparity narrowed down to a more limited variety of venation trait-combinations. It was only after the Cretaceous-Paleogene mass extinction (ca. 66 Mya) that the disparity started to increase a second time – following the diversification of extant angiosperm lineages. A subsequent analysis of the temporal dynamics in disparity for each separate clade (**Extended Data Fig. 4**) showed that (1) in eudicot clades, especially monocots, disparity consistently increased over time, and (2) in ferns, disparity plateaued ca. 200 Mya (**Extended Data Fig. 4**). Those trends were similar in both gradual (**Extended Data Fig. 4**) and punctuated (**Supplementary Fig. 2**) models of evolution.

Overall, our findings not only highlight the higher diversity of venation architectures explored by early-diverging and now-extinct fern and gymnosperm species (**Extended Data Fig. 5**), but also suggest that present-day lineages of angiosperms are still undergoing a second wave of diversification in venation architecture (i.e., no saturation of morphospace).

Correlations between climate, herbivory and venation evolution.

We compared the reconstructed temporal trajectories in venation traits and disparity metrics, with published time-series of paleoclimate (i.e., temperature[17] and atmospheric CO_2[18]) and herbivory proxy variables (i.e., global insect diversification rates)[19] (**Fig.6**). Although it is true that most insects are not phytophagous (ca. 25–35% of insect species are herbivores), previous studies have indicated herbivory as a major driver of insect diversification in many major insect orders[19], so in the absence of data on diversification rates solely for phytophagous insects, we used global rates of diversification for all major insect groups as a proxy for insect herbivory pressure. Using generalized least squares regression, a positive relationship was observed between morphospace disparity (median of centroids), and certain venation traits (*VD*, *CR*, *MST*) in small and medium vein sizes with global insect diversification rates (**Extended Data Fig. 6**). Additional regression analysis showed no evidence that the presence of leaf exudates (i.e., resins and latex) influence these correlations (see **Supplementary Note 2**). However, we found no significant correlation between venation traits and the climatic proxies investigated (**Supplementary Data 6**), except for a weak relationship between CO_2 concentrations and *CR* in gymnosperms (**Supplementary Fig. 3**). Our regression results also showed no evidence of a

significant interaction between CO_2 and temperature in influencing venation traits over time, except for *MST* (**Supplementary Data 6**). Interestingly, our temporal analysis also showed that the Late Devonian and the Triassic-Jurassic mass extinctions were not associated with major impacts on venation evolution, whereas the Permian-Triassic event was associated with significant decline in venation trait values, particularly at small vein sizes (**Fig. 6 a-c**).

These results underscore the complex multidimensional drivers of venation architecture evolution, and highlight a potential role of insect herbivory pressure on the evolution of different architecture designs. These results also show that over larger temporal or phylogenetic scales, previously reported single-variable trait-climate relationships become weak (e.g., vein density and temperature).

Discussion

Using a dataset of 1,000 (extant and extinct) species' venation networks and recently developed methods for extracting multiscale venation traits[3,19] and performing ancestral state reconstructions[16], we reconstructed the ca. 400 Myr history of leaf venation architecture evolution. Our major findings were (1) venation networks evolved from initially having fewer veins with corrugated loops, to having more veins, smoother loops (**Fig. 3a)**, and more internal free-ending veins (**Supplementary Note 1**); (2) the evolution of venation architectural designs followed a biphasic trajectory, with ferns and early-diverging seed plants first filling the boundaries of viable trait-combinations, and then with angiosperm lineages bringing architectural innovations that initiated a second and ongoing phase of interior morphospace exploration (**Fig. 5d**); and (3) insect diversification rate was correlated with venation traits over time, suggesting that biotic interactions could have been an important factor influencing venation architecture diversification over time (**Fig. 6**). These results provide a clearer understanding of leaf evolution in several areas that we explore further below.

Evolution of venation networks beyond minor vein density.

Independent evolution of highly dense vein networks (in magnoliids, monocots, and eudicots) has been documented before in studies using smaller datasets (N=307-504), consisting mostly of angiosperm species[1,7,8]. Likewise, previous studies using stratigraphic distributions and

qualitative venation characteristics have proposed a repeated differentiation from single-veined networks, to dichotomously branching, to looping networks with free-ending veins, both in ferns and seed plant lineages, via convergent evolution[9]. Here, we re-evaluated those results using quantitative multiscale venation traits combined with modern phylogenetic comparative methods[16,20] applied to a wider phylogenetic tree (N = 1,000 taxa). We not only confirmed the existence of directional trends in vein density and other important traits, but also, for the first time, showed that temporal changes in small and medium veins – but not in larger veins – were responsible for those evolutionary trends (**Fig. 3**). At least for the four venation traits evaluated here, we found no evidence of slower evolution in larger veins (**Extended Data Fig. 1**). In fact, for some traits (i.e., *ER* and *CR*) evolutionary rates were even higher (not lower) in larger veins. Therefore, the absence of directional changes in larger veins might not be linked to a lower evolutionary lability, rather it may stem from developmental or biophysical constraints. Unlike the minor veins, which are formed throughout the rapid leaf expansion phase and can develop into a wide range of final vein densities and architectures, the major veins are formed earlier during leaf development and are constrained to a narrower variety of forms, which are more strictly dependent on the total leaf area[2,21].

Multiple possible selective forces for venation evolution.

These findings for directional temporal trends, open questions about the underlying selective forces for leaf veins evolution. One possibility is that leaf networks evolved towards architectural traits linked to higher flow efficiency, at least in angiosperm lineages, as previously proposed[1,7,22]. In modern plants, these traits are key determinants of leaf hydraulic capacity. They influence plant transpiration and photosynthetic rates[2] because a larger density of smaller veins, including free-ending veins, decreases the distance of transport through the mesophyll and thereby decreases the overall hydraulic resistance of the leaf[23]. Additionally, network traits might have evolved to support other critical leaf functions, including mechanical support, resistance, and resilience to damage[3,4,24,25]. For example, a higher density of small veins may provide an advantage against herbivory, forcing insects to expend more energy to cut through more veins, and may also provide redundant pathways to bypass damaged areas[26]. This idea is corroborated by our finding of a consistent relationship between insect diversification rates and venation traits over time, suggesting that herbivory pressure could have been a potential driver of venation

architecture diversification (see below) - although further studies are needed to test this hypothesis. Although the functional significance of loop circularity ratio (*CR*) is yet to be determined[3,24], the network evolution towards smoother loops in small and medium vein sizes reflect a decrease in the relative allocation of vein perimeter relative to loop area over time[24]. This trend in CR_{small} and CR_{medium} could have led to a reduction in the surface area for water exchange between minor veins and the mesophyll, but was likely compensated by the simultaneous increase in the proportion of free-ending veins. This may suggest that free-ending veins, rather than more corrugated loops, provide a more efficient connection for water flow from the terminal xylem to the mesophyll[27].

Expansions and contractions in the venation morphospace.

The first 200 Myr of venation evolution was characterized by a gradual expansion of the morphospace, with ferns and gymnosperms slowly exploring new architectures (**Fig. 5d**), e.g., ranging from dichotomizing to looping networks, and from single-vein order to hierarchical networks (with two or more distinct vein sizes or orders, see examples in **Extended Data Fig. 5**). By the Triassic-Jurassic boundary, disparity reached its maximum value and then stabilized, likely because these non-flowering plants reached the limits of morphological and developmental variation for leaf venation under marginal leaf growth (i.e., where cell divisions are restricted to the leaf margins)[9]. During the Cretaceous, amidst the Cretaceous Terrestrial Revolution when the Earth witnessed a rapid phylogenetic divergence of angiosperm families[15], disparity decreased rapidly. Two distinct processes could have been responsible for that decline in the diversity of venation architectures. First, a sudden increase in the extinction rates of ferns in the Late Cretaceous led to a collapse in fern diversity, resulting in a loss of architectural designs that were unique to this group[25]. Second, the rise of angiosperms catalyzed a shift from plants with leaf-borne reproductive structures to plants where the reproductive and vegetative functions were segregated into separate structures, and a transition from marginal to diffuse leaf growth (i.e., where cell divisions are dispersed throughout the leaf). Those functional and developmental changes may have led to a greater functional specialization, and thereby a reduction in the diversity of venation patterns (i.e., narrowing in the morphospace occupation) in seed plants[10,28,29]. That is, with the advent of angiosperms, network diversification occurred within a more limited range of the morphospace with a high-fitness trait-combination. Simultaneously,

some of the more extreme architectures (at the morphospace edges) of non-flowering plants may no longer have been competitive and eventually disappeared (e.g., the extinct pteridosperms), even though other extreme architectures were retained until the present time (e.g., *Ginkgo*). It was only after the Cretaceous-Paleogene mass extinction that the disparity in venation architecture started increasing again in tandem with the radiation of extant angiosperms lineages[30,31]. Those new lineages developed the complex architectural designs dominant in the modern world, characterized by hierarchical orders of reticulate veins (i.e., loops within loops) and dispersed, internal free-vein endings. Although similar architectural designs have evolved at least three times in non-angiosperm seed plants (e.g., Gnetales and Gigantopterids) and at least ten times among extant ferns (e.g., Dipterids and Polypods)[9], it was only in those later-diverging angiosperms lineages that hierarchical reticulate networks became common. This is likely because the late angiosperm transitions from tracheids to xylem vessels[7,32], and from scalariform to simple perforation plates[33], reduced the resistance to water flow inside the venation system, thus allowing the miniaturization of veins[7] and the development of more and more complex networks. Notably, the development of the 'striate' parallel venation, typical of monocots, which is composed of several orders of longitudinal veins with small transverse veins connecting them[34], allowed eudicot plants to explore novel areas of morphospace, also largely contributing to the increase in disparity from the Cenozoic towards the present. An increase in disparity followed by a saturation of morphological potential is a common evolutionary pattern, observed both in plants and animals[35,36]. The fact that the second phase of increasing disparity in vascular plants has still not leveled off suggests that extant plant lineages have yet to explore new viable trait-combinations.

Linkages between vein evolution, herbivory, and climate.

Despite the known mechanistic feedbacks between plants, CO_2 concentrations, and temperature[37] mediated by vein density and other venation traits[24], we found no evidence of a strong relationship between venation traits and those climatic factors over time, neither for vascular plants as a whole, nor for each clade separately. For example, although global CO_2 concentrations and temperatures fluctuated widely during the first 250 Myr of vascular plant evolution, vein density and other venation traits remained relatively unchanged over this period. Because CO_2 and temperature fluctuations may interact with other important environmental

342 factors (e.g., precipitation amount and seasonality) not considered in this study, it may be hard to
343 disentangle the individual effect of climatic factors on venation trait evolution.
344
345 Instead of being spurred by changes in climatic conditions, the evolutionary transformations
346 observed in venation architecture could have been a response to altered herbivory pressure, as
347 suggested by the association found in this study between different venation traits and global
348 insect diversification rates. Insects and plants have been interacting since their origins, with those
349 interactions driving the evolution of a notable taxonomic diversity in both groups[38]. Because
350 80% of herbivory damage in terms of leaf biomass is carried out by insects[39], an increase in the
351 diversity and abundance of phytophagous insects could have imposed selection on leaves for
352 higher resistance or resilience to damage. This could have been achieved, for example, by
353 developing more veins (so insects would spend more energy cutting through veins[2]) and/or more
354 loops (so water or latex could flow around damaged areas[14]). Here, we were not able to
355 differentiate the diversification rates of phytophagous versus non-phytophagous insects. We also
356 did not consider evolutionary rates of other herbivores such as dinosaurs or mammals, but they
357 might also be important for venation evolution.
358
359 Our broad-scale correlational study cannot conclusively support or reject any of these
360 hypotheses, but highlights the value of further investigating each. It is also possible that observed
361 correlations between variables are caused by an unmeasured third variable. For example, minor
362 vein density increased with angiosperm diversification and this could have been coupled with
363 insect diversification via insect-plant pollination coevolution, rather than by insect herbivory (but
364 see [40]). Additionally, insect herbivory could have been an incidental influence on leaf venation
365 evolution when compared to other factors driving venation evolution (e.g., related to
366 photosynthetic machinery, stomata), particularly because resistance or resilience to herbivory
367 damage can be achieved by a range of adaptations, such as chemical defenses (e.g., secondary
368 metabolites) and morphological barriers (e.g., trichomes and spines), that are independent of
369 venation traits[41]. Therefore, further studies examining how changes in venation traits are related
370 to insect damage observed across the fossil leaf record[38], will be crucial to elucidate to what
371 extent the correlations observed here reflect causal links between the diversification of insects

and venation networks. Nevertheless, our dataset provides a first resource for future tests of biotic vs. abiotic factors influencing network evolution.

Conclusions.

This study provided an updated and data-rich perspective on leaf venation networks over 400 Myr of time. It demonstrated the contingency, complexity, scale-dependence, and nonlinearity of the evolutionary process, building a more detailed understanding of plant evolution relative to prior studies [1,8,23]. The hypotheses and correlations identified here, especially around herbivore evolution, will require further assessment but highlight the diversity of factors that may have shaped leaf evolution.

Online Methods

Obtaining images of leaf venation networks.

We compiled 1,000 leaf images of extant (N = 880) and fossil (N = 120) species, distributed in 784 genera, 325 families, and 90 orders (**Supplementary Data 7**). To create this unique dataset, we brought together samples from multiple collections.

Images of extant species were selected from: (1) Smithsonian National Cleared Leaf Collection: comprises 7,000 images available at https://collections.peabody.yale.edu/pb/nclc/; (2) University of California Museum of Paleontology (UCMP) Cleared Leaf Collection: comprises over 2,000 samples, including the Daniel I. Axelrod collection. Low-resolution images of some samples are available at (https://ucmp.berkeley.edu/collections/paleobotany-collection/). Other samples were were imaged at high resolution for this study; (3) Wilf collection[42]: an open-access database of 26,176 leaf images; and (4) Macrosystem Ecology Laboratory at Berkeley (MEL) collection: a database of 326 leaf images collected from Costa Rica, Ghana, Ecuador, and United States, including the University of California Botanical Garden at Berkeley (UCBG). Our previous work[43,44] provides a full description of how MEL leaf samples were collected, cleared, and imaged.

We evaluated all leaf images from these collections to determine which samples were suitable for our work. We selected only high-contrast and resolution images showing the whole leaf or

with at least 75% of the leaf area present, and with no major damage (e.g., tears, holes, folds, bubbles, herbivory, or material deterioration). For many monocot species, leaves were too long (>30 cm) to be wholly imaged, so a leaf segment representing ca. 20-50% of the total leaf area was analyzed. Notably, due to the variable resolution of the leaf images, our study was able to accurately resolve any vein with width ≥10 □m, but occasionally missed small veins.

Images of extinct species were compiled from compression leaf fossil images from: (1) Yale Peabody Museum (https://peabody.yale.edu/): 4,300 imaged specimens, including Triassic and late Cretaceous floras from Arizona, New York, New Jersey, and southern New England, available at GBIF (www.gbif.org); (2) Natural History Museum of Berlin (https://www.museumfuernaturkunde.berlin/): 29,826 fossil records from the Paleozoic to Cenozoic eras, available at GBIF too; (3) University of California Museum of Paleontology: ca. 12,000 fossil specimens available at https://ucmpdb.berkeley.edu/. (4) Illinois State Museum (https://www.illinoisstatemuseum.org/): 600 samples, including many Carboniferous fossils from the Mazon Creek formation; (5) Florida Museum (https://www.floridamuseum.ufl.edu/): ca. 250,000 specimens, ranging from the Proterozoic to the Pleistocene; and (6) University of Alberta Paleobotanical Collection: ca. 127,000 fossil specimens, available at https://search.museums.ualberta.ca/. In addition to those museum collections, we also sampled images of fossil leaves from the Wilf collection[42], which compiled 4,076 samples dated from Late Cretaceous to Eocene, including specimens from the Florissant Fossil Beds National Monument (late Eocene, Colorado, US). Although leaf fossils are abundant in many depositional settings, the preservation of whole-leaf venation networks in fossils is rare. Thus, instead of whole leaves, we sampled leaf sections (ranging from 19 to 32,000 mm^2) from any leaf fossil image where tertiary or smaller veins were distinguishable. We also only retained fossil samples whose taxonomic identity and age could be retrieved, as this information was required for grafting fossil taxa to the phylogenetic tree (see 'Obtaining phylogenetic tree' section). After inspecting all fossil images from these databases, we noticed an absence of samples from the Jurassic period. To fill this gap, we conducted a targeted literature search on the 'Google scholar' database using the key-words "Jurassic leaf fossil*", and found seven peer-reviewed papers[1] from which we extracted 20 traceable leaf fossil images. We recognize that our survey of fossils is not exhaustive, and it is potentially biased towards taxa more likely to fossilize well. For

example, the fossil record is biased against the preservation of taxa with low leaf mass per area, as these leaves tend to be mechanically damaged before fossilization [52]. Because low leaf mass per area can be linked to lower vein density, particularly of larger veins [3], VD_{large} could be underrepresented in our fossil dataset. Despite those limitations, our fossil dataset yielded key coverage of important internal nodes, ranging in age from 11.6 to 358.9 Mya, the time period of vascular land plant evolution.

When compiling leaf images, we aimed to maximize phylogenetic coverage, by sampling species from all major vascular plant clades, including: (1) ferns, (2) gymnosperms (including Bennettitales, Caytoniales, Cordaitanthales, Medullosales), (3) basal angiosperms (including Amborellales, Nymphaeales, Austrobaileyales, Chloranthales, and Magnoliids), (4) monocots (including Commelinids), (5) basal eudicots (including Ranunculales, Proteales, Trochodendrales, Buxales, Gunnerales, Dilleniales, Saxifragales), (6) rosids, and (7) asterids. We limited our analysis to one leaf per species, so our study does not address trait intraspecific variation. This approach is justified since our study focuses on interspecific trait variation across the plant phylogeny.

Obtaining the phylogenetic tree of extant and fossil taxa.

We assembled a time-calibrated phylogenetic supertree for all 1,000 vascular plant species evaluated in this study (**Fig. 1**, **Supplementary Fig. 1**). First, we used the R-package 'U.Taxostand'[53] to standardize spellings and nomenclature for all extant species names, following the World Plants (worldplants.de) database and the APG IV classification[54]. Similarly, fossil names were standardized following the Paleobiology (paleobiodb.org) and Fossilworks (fossilworks.org) databases. After nomenclature standardization, we built a phylogenetic tree for all extant species using the 'V.PhyloMaker2' R-package[55] and the 'GBOTB.extended.WP.tre' mega-tree.

Next, to graft our fossil species to the tree, we used the function 'tree.merger' from the 'RRphylo' R-package[20]. This function allows adding individual species (i.e., our fossil species) to a backbone phylogeny (i.e., our phylogenetic tree of extant species), while also automatically recalibrating the tree based on age values provided for specific nodes and/or tips (i.e., fossil species last appearance age). To properly attach the fossil species, the 'tree.merger' function

requires: (1) name of the fossil species; (2) fossil's sister taxon(a) (i.e., the fossil closest relative(s) present in the pre-existing tree); (3) fossil estimated last appearance age; and, optionally, (4) the estimated age of the parent node (i.e., age of the node the fossil species descend from). For example, the backbone tree included the extant species *Betula occidentalis*, so the fossil species *B. leopoldae* was grafted in this same genus, and all its parent nodes were recalibrated to consider the fossil species last appearance age at 38 Mya (see **Supplementary Data 8**).

The information necessary for fossil grafting was obtained from the Paleobiology and Fossilworks databases, and the tree root age was placed in the Devonian, at 400.78 Mya. The ages of the internal nodes encompassing each of our seven major plant clades were also recalibrated using median estimated ages extracted from "TimeTree" database[56]. In a few cases, information in those databases were outdated, and replaced with split age estimates reported in more recent sources[57]. All information used for fossil grafting and tree calibration are available in **Supplementary Data 8**. Uncertainty in tips and node ages were later accounted for in our analysis (see "Identifying macroevolutionary trends" section) via bootstrapping methods using the "overfitRR" function[58] from the "RRphylo" R-package.

Extracting venation architectural traits.

We used GIMP version 2.10.32 (https://www.gimp.org/downloads/) and ImageJ version 1.53t (https://imagej.nih.gov/) to pre-process all leaf images. Image pre-processing involved cropping the leaf image, preparing masks to delineate leaf boundaries, and determining image resolution, which ranged from 0.003 to 0.061 pixels mm^{-1} in extant species and from 0.006 to 0.179 pixels mm^{-1} in fossil species (**Supplementary Data 7**). For some species with a large midrib (i.e., midvein), a mask of the midrib was also prepared to prevent it from splitting into multiple segments during the network extraction. After pre-processing, leaf image segmentation (i.e., conversion of a coloured leaf cleared image into a binary image where veins pixels are shown in white and non-veins pixels are shown in black) was done automatically using LeafVeinCNN program versions 1.0.7[59] and 2.12[43]. We configured LeafVeinCNN to use an ensemble average of three convolutional neural network predictions (CNNs) to segment veins. For leaf images that did not have a good color-contrast or had parallel venation type, the CNNs sometimes failed to properly segment the veins. In those cases (N = 25), we manually hand-traced the venation

network using GIMP. Since our CNNs were not trained to segment fossil images, all leaf fossil samples were carefully hand-traced in GIMP by a trained expert. All tracings were error-checked by at least two other experts prior to finalization. There is some remaining uncertainty in the accuracy of tracings due to the low resolution of some fossil images or imperfect preservation of fossil samples. These issues primarily affect the smaller veins.

The segmentation process resulted in over 19 million veins segmented and resolved veins with width ≥10 □m. All segmented venation networks were then processed in the LeafVeinCNN program to (1) produce a spatial graph representation of the entire venation network (i.e., to convert a binary image into a spatial graph where veins are represented by segments of known length and width connected to each other by nodes), (2) generate hierarchical loop decompositions[26,59] (i.e., to map a loopy network to a binary tree by sequentially fusing and deleting looping veins of similar diameter), and (3) calculate a series of multiscale venation statistics that describes how the venation network topology and geometry change across vein sizes. Here, we focused on four multiscale traits (**Fig. 2**): vein density (*VD*), minimum spanning tree ratio (*MST*), loop elongation ratio (*ER*), and circularity ratio (*CR*). *VD* was calculated as the ratio between all vein segments (in mm) and the one-sided leaf total area (in mm^2). *MST* was calculated by computing the length of the minimum spanning tree (i.e., tree that connects all the vein junctions, without creating any loops and with the minimum possible total length) divided by the length of all veins. *ER* was calculated by fitting an ellipse to each loop, and dividing the major axis length by the minor axis length, then taking the median ratio across all loops. *CR* was calculated by dividing the loop area by the squared loop perimeter for each loop, then multiplying by 4π, then taking the median value across all loops. To minimize undersampling biases of large veins, we truncated those four multiscale statistics to the 0.01– 1.5 mm range of vein width, though larger veins were present (**Supplementary Fig. 4**). Although those four venation traits have been identified as key traits to capture leading axes of variation in network architecture across many species[3,60], we recognize that other network single-scale (e.g., branching angles and connectivity), cross-scale (e.g., tapering of veins), and qualitative metrics (e.g., pinnate vs palmate) could be important to fully characterize the diversity of architectural designs.

Identifying evolutionary trends in venation traits.

We investigated how *VD*, *MST*, *ER*, *CR* varied over time at each vein spatial scale (small, medium, large sizes). To make an interpretable assessment of trait evolution at different vein spatial scales we binned vein trait values for each species at three size classes. Because the range of vein widths largely vary across leaf samples (i.e., a vein with 0.3 mm width can be a primary vein in a small leaf, but a tertiary vein in a large leaf) and some samples exhibit vein tapering (i.e., veins become gradually smaller), there was no easy way to use machine-classifiable algorithms to assign each segmented vein to a specific vein order (e.g., primary, secondary, and tertiary vein classes). Thus, instead of using vein orders, we classified vein widths into three size classes based on their relative sizes (see **Extended Data Fig.2**). Therefore, our study prioritized greater taxonomic and whole-leaf coverage at the expense of developmental precision in vein classification. To classify veins into vein sizes classes, we first standardized (z-transformed) vein width values for each species, by dividing each vein width by the maximum width value of that species. Therefore, scaled vein sizes varied between 0 and 1 across all species. Next, for each species we classified vein sizes into small ($0 <$ scaled vein width ≤ 0.3), medium ($0.3 <$ scaled vein width ≤ 0.6), and large (scaled vein width > 0.6 mm) classes.

We used the 'RRphylo' R-package[16] to investigate the rates and trajectories of diversification over time in each of our four architecture traits at each vein size. 'RRphylo' performs a phylogenetic ridge regression (a maximum-likelihood method) on a phylogenetic tree and associated trait data to return both the ancestral estimates at internal nodes and the branch-wise rates of trait evolution[61]. Those rates are phylogenetic ridge regression coefficients (i.e., represent the trait change per unit time between consecutive nodes in the tree), so they have both a direction (indicating whether the mean trait value increases or decreases over time) and a magnitude (indicating the speed of mean trait value change over time). 'RRphylo' assumes no specific *a priori* evolutionary model about the tempo and mode of trait evolution. It is also specifically designed to process phylogenies including fossil species (i.e., fossil trait information is directly integrated in the ancestral state reconstruction), which improves, and in some cases even changes, our understanding of trait evolution[60].

To test for the existence of evolutionary trends (i.e., directional patterns of evolutionary trait mean change over time) in venation architecture, we applied the function 'search.trend' from 'RRphylo' for each trait at each vein class. This function first performs a linear phylogenetic ridge regression between trait values (obtained by collating ancestral state estimates to measured trait values at the tree tips) and evolutionary rates (trait change per unit time between consecutive nodes in the tree) versus ages (their distance from the tree root). A potential limitation of this approach is that only linear associations are considered, i.e., non-linear trends in single-traits were not examined here. Significance of the linear evolutionary trends was assessed as the probability that those linear regression slopes differ from a family of 100 regression slopes ('BMslopes') generated according to the Brownian motion (BM) model of evolution. In the BM simulations, species mean trait values are assumed to evolve through a flat adaptive landscape, i.e., the evolutionary changes along branches in the tree have an expected value of zero and are normally distributed with a variance proportional to the length of the branch. A significant evolutionary trend exists whenever the trait regression slopes significantly depart from the BMslopes simulations. Therefore, for a two-tailed test at $\alpha = 0.05$, significant trends exist whenever p.random < 0.05 (significant decrease in rates or trait means over time) or p.random > 0.95 (significant increase). The 'search.trend' function was used to identify evolutionary trends both on vascular plants as a whole (i.e., for the entire plant phylogeny) and on each focal clade individually. In the latter case, clades presumed to experience trended evolution must be indicated by their nodes. Because in our tree the clade basal eudicots constitute a paraphyletic group (see **Fig.1**), we ran 'search.trend' function separately for the order Ranunculales (basal eudicots 1), Proteales (basal eudicots 2), and Saxifragales (basal eudicots 3). Following recent analysis based on nuclear data[62], we placed the orders Santalales, Berberidopsidales, and Caryophyllales in the asterid clade ("superasterids"). All p-values generated using the 'search.trend' function were adjusted using the Benjamini and Hochberg[63] correction, as implemented in the R-function 'p.adjust'.

To assess whether the evolutionary trends identified were robust to sampling and phylogenetic uncertainty, we applied the 'overfitRR*'* function from the 'RRphylo' R-package[58]. This function randomly removes a number of species corresponding to ca. 25% of the tree size, swaps the phylogenetic position of ca. 15% of tips (tips are swapped across up to two nodes), and 'moves'

589 in time 15% of the tree nodes (nodes are changed in age between the age of its ancestor and the
590 age of its daughter node). Then, it performs 'search.trend' on the new tree and data. This
591 procedure is repeated 100 times and the percentage of significant results is returned. The
592 'overfitRR' function also regresses the original ancestral reconstructed states at internal nodes
593 with the states produced after each subsampling and swapping. Regression slopes close to 1
594 indicate a closer match between original and resampled values, suggesting more robust
595 estimation[58].
596
597 To test for statistically significant differences among the venation traits evolutionary rates across
598 vein sizes, we used Wilcoxon-tests, as implemented in the R-package 'rstatix'. To facilitate
599 comparisons across vein sizes and across different venation traits, Wilcoxon-tests were
600 conducted on the absolute log-transformed evolutionary rates obtained with the 'RRphylo'
601 approach described in the section above.
602
603 ***Disparity through time analysis.***
604 To investigate in which clades the evolution of novel architectural trait-combinations have
605 originated and how the diversity of architectures varied over time we performed a disparity
606 (multidimensional space occupancy) analysis using the 'dispRity' R-package[64]. First, we carried
607 out a principal component analysis (PCA) across the four venation traits at each vein class to
608 define the multidimensional venation architectural space (morphospace). PCA was run by
609 collating ancestral state estimates at internal nodes to trait values measured at the tree tips. Prior
610 to PCA, all traits were centered and scaled (z-transformed) to improve comparability among
611 them and to reduce bias towards traits with higher variance. *VD* and *ER* values were also square-
612 root-transformed to improve normality. Using this 12-dimensional architectural space, we
613 calculated two metrics of disparity describing complementary aspects of the multidimensional
614 space occupancy: (1) the median centroids - equation (1), the median distance between each
615 element and the centroid of the ordinated space, which describe the position of an element in the
616 morphospace compared to a fixed point in this space (i.e., the space centroid); and (2) the sum
617 variances - equation (2), the sum of variance of each dimension of the ordinated space, which
618 characterizes the size of morphospace occupied by each element[63].
619

□□□□□□□□□□ = $\sqrt{\sum_{□=1}^{□} (□_{□} - □□□□□□□□□_{□})^2}$ **Equation (1)**

□□□□□□□□□□ = $□^2$ $□_{□}$ **Equation (2)**

Where *d* is the number of dimensions, *n* the number of elements, σ 2 is the variance of each dimension, *i* is any row of the data.

To test whether different clades occupy different regions of the architectural space, we used the function 'dispRity.per.group', which measured the disparity between each clade. To make each time-slice more robust to outliers, we used the 'boot.matrix' function which pseudo-replicate the (PCA) ordination matrix used for the disparity measurements 100 times to see how sensitive they are to outliers in the dataset. Significant differences in morphospace occupation among clades were then tested using the 'test.dispRity' function, which performed a nonparametric multivariate analysis of variance (NPMANOVA) followed by post-hoc t-test with Bonferroni p-value correction.

To test how the space occupancy varied across time (e.g., test whether the disparity metrics increased or decreased over time), we used the 'dispRity.through.time' function[64] to conduct a disparity-through-time (DTT) analyses using the time-slicing method[65]. Unlike other DTT methods based on time-binning, time-slicing (continuous time subsets) uses a time-calibrated phylogenetic tree and considers subsets of taxa at specific equidistant points in time, which results in even-sampling across time and allows the definition of the underlying model of character evolution (punctuated or gradual evolution). As we did not have an *a priori* hypothesis for the model of venation architecture evolution, we performed the time-slicing using two alternative models: a punctuated model (i.e., "proximity") and a gradual model (i.e., "gradual.splits") of evolution[65]. Those model arguments ("proximity" or "gradual.splits") are used when the time slice occurs along a branch of the tree rather than on a tip or a node, meaning that a decision must be made about what the value for the branch should be. In both time-slicing models, we divided the ca. 400 Myr time-frame of vascular plant evolution into 40 time-slices of ca. 10 Myr of duration each. Extant taxa were split inside each time-slice according to their age (taxa were considered as single points in time). To account for the uncertainty in the fossil ages, the first and last occurrence data for each fossil taxon was used during the time-slicing process, so those taxa could appear in more than one time-slice. To make each time-slice more robust to

outliers, we used the 'boot.matrix' function to perform 100 bootstrapping iterations in the PCA dataset. Next, we used the function 'test.dispRity' to test for significant changes in disparity over time using Wilcoxon-test applied to time-sliced disparity with sequential comparisons and Bonferroni p-value correction. DTT analysis was performed both for the entire dataset (all 1,000 species together), and for each clade separately. In the latter case, we first used the function 'extract.clade' from the 'ape' R-package to extract a subtree for each clade, then we conducted the DTT analysis on each of those subtrees. The number of time-slices used varied among clades, and was determined by dividing the root tree age by 10, so for all clades each time-slice had a fixed duration of ca.10 Myr.

Finally, we also quantified the evolutionary mode of venation architecture diversification by using the 'model.test' function to fit five alternative modes of disparity changes through time: (1) Stasis (time-invariant change: null expectation of time-invariant change in disparity in which disparity values fluctuate with a variance around the mean); (2) Brownian-motion model (BM - random-walk: assumes a constant mean that is equal to the ancestral estimate of the sequence, and the variance around this mean increases linearly with time); (3) Ornstein-Uhlenbeck (OU - evolution constrained to an optima); (4) Trend (increasing or decreasing mean through time); and (5) Early Burst (EB - exponentially decreasing rate through time). The goodness of fit of each candidate evolutionary model was then determined using AIC (Akaike Information Criterion) scores, and the model with lowest AIC was selected as the best.

Associations between venation, biotic, and abiotic proxies.

To explore abiotic and biotic factors that may have influenced leaf venation evolution in vascular plants, we compared the reconstructed evolutionary trajectories of single venation traits and the patterns of venation architectural disparity with global average temperature[17], atmospheric CO_2 concentration[18], and global insect diversification rates[19] for the Phanerozoic eon. In the absence of global insect diversification rates for phytophagous versus non-phytophagous insects, we assumed those rates to be consistent with each other, as for the majority of insect orders a strong and positive relationship exists between herbivory and diversification rates [40]. Time-binned median values of each of these time-series data sets were calculated (at ca. 10 Myr bins for the pooled regressions or at ca. 2 Myr bins for the individual clade regressions) and used in the

regression analyses. To test for temporal autocorrelation in our datasets, we first ran multivariate ordinary least square (OLS) regressions between each response variable (VD_{small}, VD_{medium}, CR_{smal}, CR_{medium}, MST_{small}, MST_{medium}, sum of variances, and median of centroids) and all our predictor variables (CO_2, temperature, and insect rates), e.g., VD_{small} ~CO_2 + temperature + insect rates. Then, we used the Durbin-Watson test to check for significant autocorrelation in the residuals of the OLS regressions. Whenever this test was significant (p-value< 0.05), we refit the model using generalized least squares (GLS) regression fitted by maximizing the restricted log-likelihood (REML) with an autocorrelation moving-average structure of order one to three (e.g., VD_{small} ~ CO_2 + temperature + insect rates, correlation = corARMA(p = n), method = "REML"; where n = 1, 2 or 3) as implemented in the R-package "nlme". This approach estimates the strength of serial correlation in the relationship between variables, correcting for the non-independence of adjacent points within a time series. Finally, we chose the GLS model with best-fit according to the AIC. To test for potential interactive effects between abiotic variables, we also ran additional models including an interaction term between CO_2 and temperature (e.g., VD_{small} ~ CO_2 * temperature + insect diversification rates) for all species pooled together. Additional regression analysis, using only Angiosperm species, were run to investigate potential compensatory effects of the presence of leaf exudates (i.e., resins and latex) on the correlation between insect diversification rates and venation traits (see **Supplementary Note 2**). Note that we only ran those time-series regression analysis for the venation traits and clades that had shown a significant evolutionary trend in accordance with the analysis described in the two sections above.

All analyses were carried out using R version 4.3.1 (R Core Team, 2023).

Data availability

Data to reproduce all analysis will be made publicly available on Zenodo (10.5281/zenodo.13300782)[66] upon acceptance of this manuscript. The original cleared leaf images, leaf masks, extracted networks, and all LeafVeinCNN outputs for the 122 leaf samples collected at the University of California Botanical Garden at Berkeley are available at doi: 10.5061/dryad.1g1jwsv36[67]. Network segmentations and leaf masks of all other 878 samples are available at 10.5281/zenodo.13300782 and 10.5281/zenodo.15217651[68], as well as high-

resolution cleared leaf images from Ecuador, Costa Rica, Ghana, and University of California Museum of Paleontology collections. Original leaf cleared images of all other extant species are available at Wilf collection https://phytokeys.pensoft.net/article/72350/, Smithsonian National Cleared Leaf Collection https://collections.peabody.yale.edu/pb/nclc/. Original fossil leaf images are publicly available at https://peabody.yale.edu/; www.gbif.org; https://www.museumfuernaturkunde.berlin/; https://ucmpdb.berkeley.edu/, https://www.floridamuseum.ufl.edu/, https://search.museums.ualberta.ca/, https://ucmp.berkeley.edu/collections/paleobotany-collection/, https://phytokeys.pensoft.net/article/72350/,https://doi.org/10.1016/j.palwor.2017.01.003, https://doi.org/10.1080/14772019.2014.936974, https://doi.org/10.1080/11035890902857846, https://doi.org/10.1016/j.revpalbo.2009.08.004, https://doi.org/10.1016/j.revpalbo.2017.08.003, https://doi.org/10.1515/acpa-2017-0012, https://api.semanticscholar.org/CorpusID:135128574. World Plants (https://worldplants.de/), Paleobiology (https://paleobiodb.org/) and Fossilworks (fossilworks.org) databases were used to standardize species names. TimeTree: the timescale of life (https://timetree.org/) database was used to recalibrate the age of internal nodes of the phylogenetic tree.

Code availability

Data and R-code to reproduce all analyses and figures are available at 10.5281/zenodo.13300782 and will be made publicly available upon acceptance of this manuscript.

Acknowledgements

This study was supported by the United States National Science Foundation (grant DEB-2025282, BB) with supplements from the Research Experience for Undergraduates (REU), Research Experience for Post-Baccalaureate Students (REPS), and Research Experience for Teachers (RET) programs, the University of California at Berkeley Sponsored Projects for Undergraduate Research (SPUR) program, and the United Kingdom Natural Environment Research Council (NE/M019160/1, MF). Ghana samples were collected under permit of the Forestry Research Institute of Ghana (FORIG, MB) at Kumasi, Ghana. Costa Rica samples were collected under permit ACOPAC-INV-RES-002-11, issued to B. Boyle by the Ministerio de Ambiente, Energía y Telecomunicaciones, Área de Conservación del Pacífico Central. Ecuador

samples were collected under Ministerio Del Ambiente permit 004-2019-IC-PNY-DPAO/AVS and exported under permit MAE-DPAO-2019-1275-O. Ecuador field sampling efforts were funded by CTFS ForestGeo grants program, and the Arizona State University WAESO program that funded the undergraduate research technicians that processed the Ecuador leaf samples. We acknowledge Peter Wilf for organizing and publishing a large image database of extant cleared and fossil leaves, and thank him for providing useful feedback on a first draft of this manuscript. We thank Silvia Castiglione and Pasquale Raia for providing input on RRphylo, and Sami Rifai for providing computational support for the bootstrapping analysis. We are grateful to all staff of the University of California Botanical Garden at Berkeley for the logistical support, especially to the horticulturists Ethan Fenner, Eric Hupperts, James Fong, Noah Gapsis, Gideon Dollarhide, Sophia Warsh, Jason Bonham, and Corina Rieder who helped us with sample collection.

Authors Contributions:

BWB, MF, LMTA and BJE acquired funding. ISM and BWB designed the study. MF developed the program for leaf venation extraction, which was improved by BWB, SS, SM, and CT, using venation images hand-traced by CP, NV, and HJP. HF and DME provided logistical support to access the University of California Botanical Garden (UCBG) living collections and the University of California Museum of Paleontology (UCMP) cleared leaf collections, respectively. IN led a lab team group responsible for clearing (SC, MA, AC, MS, NY) and imaging (AE) the UCBG leaf samples. LMTA, EGH, REC, MR and MAD collected and prepared the Ecuador leaf samples. MB collected the Ghana leaf samples. BB collected the Costa Rica leaf samples with funding from BJE. EGH collected the Ecuador leaf samples with funding from LMTA. EX selected and imaged the UCMP leaf samples. BV, JM, NV, MB, ISM, and CP hand-traced leaf images and prepared leaf masks of extant species, while MBF, RJW, and JL hand-traced fossil leaf images. BV, JM, MS, and ISM used the LeafVeinCNN program to extract the leaf venation networks and the leaf architectural traits. KD provided critical support for the data analysis. ISM analyzed the data and drafted the manuscript. All authors contributed to and revised the manuscript.

Competing Interests Statement:

The authors declare that they have no competing interests.

Tables: NA

Figure Legends/Captions (for main text figures):

Fig. 1: Time-calibrated phylogeny of 1,000 vascular plant taxa. Red branches indicate fossil taxa (N = 120), while black branches indicate extant taxa (N = 880). The other colored branches indicate the taxa depicted in the outer images. Parenthetical numbers indicate the number of extant (black) and fossil (red) taxa sampled in each clade. Internal nodes for each clade are indicated by the labeled, colored rectangles. The colors of the outer circles represent the clades depicted in the caption. The outer images are representative of taxa with distinct leaf venation network architectures. a, Microlepia platyphylla (Dennstaedtiaceae). b, Onoclea sensibilis (Onocleaceae). c, Gnetum nodiflorum (Gnetaceae). d, Agathis lanceolata (Araucariaceae). e, Tasmannia lanceolata (Winteraceae). f, Umbellularia californica (Lauraceae). g, Barbacenia purpurea (Velloziaceae). h, Smilax hispida (Smilacaceae). i, Pollia crispata (Commelinaceae). j, Parvatia brunoniana (Lardizabalaceae). k, Synaphea dilatata (Proteaceae). l, Buxus harlandii (Buxaceae). m, Ungnadia speciosa (Sapindaceae). n, Luehea tessmannii (Malvaceae). o, Hua gabonii (Huaceae). p, Aextoxicon punctatum (Aextoxicaceae). q, Grenacheria beccariana (Primulaceae). r, Cavendishia guatemalensis (Ericaceae). s, Guettarda seabra (Rubiaceae). t, Phelline brachyphylla (Phellinaceae). Note that in our analyses basal eudicots comprise three monophyletic groups (b.eu1-b.eu3). All gray scale bars represent 5 mm. Supplementary Fig. 1 shows this tree with visible taxon names and node labels.

Fig. 2: Examples of leaf networks with low and high values for four architecture traits. a, Vein density (VD, mm mm-2): quantifies the length of total vein segments per unit of leaf area, i.e., if leaf networks have fewer (low VD) or more (high VD) veins per area. b, Minimum spanning tree ratio (MST, dimensionless): describes the degree of reticulation or branching, i.e., whether leaf networks have more loops (low MST) or fewer loops (high MST). c, Loop elongation ratio (ER, dimensionless): describes the shape of the loops, i.e., if loops are more circular (low ER) or more elongated (high ER). d, Loop circularity ratio (CR, dimensionless): describes the degree of loop smoothness, i.e., if loops are more (low CR) or less smooth (high CR). All illustrations show networks with high or low values of each venation architecture trait across three vein size scales

(large, medium, and small vein sizes). However, architecture traits can also vary independently across scales, e.g., a network can have branching large veins with low density, but looping small veins with high density. These size classification into small, medium, and large veins do not necessarily coincide with vein orders (e.g., primary, secondary, tertiary).

Fig. 3: Evolutionary trends in four leaf venation architecture traits across vein sizes (small, medium, large) for the entire phylogeny of vascular plants. a, Summary of the overall evolutionary trends of venation architectural traits; b, Vein density (VD, mm mm-2); c, Minimum spanning tree ratio (MST, dimensionless); d, Loop elongation ratio (ER, dimensionless); e, Loop circularity ratio (CR, dimensionless). Points represent measured trait values at phylogenetic tree tips and maximum likelihood ancestral state estimates of internal nodes. Lines show phylogenetic ridge regression estimates of linear trends in mean trait values over time. An '*' on the right side indicates a significant trend ($\alpha = 0.05$). Insets illustrate the significant trends. Insets were not included for ER, since no significant directional trend was detected for this trait.

Fig. 4: Evolutionary trends in individual leaf venation architecture traits across vein sizes and plant clades. a-c, Vein density (VD); d-f, Minimum spanning tree ratio (MST); g-i, Loop elongation ratio (ER); j-l, Loop circularity ratio (CR). Red circles represent actual trait values, while gray circles represent internal nodes ancestral state estimates. The regression of mean trait values through time for all clades together is indicated by a black solid line. A * indicates significant evolutionary trends for the clade of that color. All venation architecture traits were rescaled to vary between 0-1 for ease of comparison.

Fig. 5: The venation architectural space of vascular plants and its variation over time. a, First (PC1) and second (PC2) principal components of leaf venation architecture traits (VD, MST, ER, CR) at three vein sizes (small, medium, large) across plant clades. Differences across plant clades in two metrics of disparity describing b, the position occupied (i.e., median centroids), and c, the extent of space occupied (i.e., sum variances). d, Temporal changes in the venation architectural space occupation under a gradual model of evolution. In panel a, venation trait values were obtained by collating ancestral state estimates to measured trait values at the tree

tips. 95% confidence ellipses enclose the data at each clade. In panel b-c, letters indicate significant difference (α = 0.05) between clades according to NPMANOVA tests. In panel d, black and red lines indicate the median disparity metric value for each ca. 10 Myr time slice and the corresponding 50% and 95% confidence intervals. The colored vertical lines indicate the approximate age of origin of each vascular plant clade. The dashed black line indicates the different phases (phases 1-4) of disparity variation over time. Note that panel a only depicts a 2-dimensional architectural space, while the two disparity metrics (in panels b-d) were calculated using the 12-dimensional space. Species depicted in panel a: 1. *Equisetum telmateia* (Equisetaceae), 2. *Puya alpestris* (Bromeliaceae), 3. *Astelia banksii* (Asteliaceae), 4. *Luzula nivea* (Juncaceae), 5. *Ginkgoites* sp. (Ginkgoaceae), 6. *Typha latissima* (Typhaceae), 7. *Nilssonia* sp. (Nilssoniaceae), 8. *Triantha glutinosa* (Tofieldiaceae), 9. *Floerkea prosperpinacoides* (Limnanthaceae), 10. *Pteridium esculetum* (Dennstaedtiaceae), 11. *Baccharis sergilioides* (Asteraceae), 12. *Sagenopteris philippsii* (Caytoniaceae), 13. *Fouquieria splendens* (Fouquieriaceae), 14. *Castanopsis chrysophylla* (Fagaceae), 15. *Colubrina glabra* (Crossosomataceae), 16. *Gnetum gnemonoides* (Gnetaceae), 17. *Beilschmiedia erythrophloea* (Lauraceae), 18. *Khaya grandifoliola* (Meliaceae), 19. *Dioscorea polystachya* (Dioscoreaceae), 20. *Cylista preussii* (Fabaceae), 21. *Hamamelis virginiana* (Hamamelidaceae), 22. *Scrophularia nodosa* (Scrophulariaceae), 23. *Fagus longifolia* (Fagaceae), 24. *Dryopteris remota* (Dryopteridaceae), 25. *Helwingia chinensis* (Aquifoliaceae), 26. *Microlepia platypoda* (Dennstaedtiaceae), 27. *Attalea rostrata* (Arecaceae).

Fig. 6: Variation in leaf venation architecture compared to abiotic and biotic proxies across the Phanerozoic eon. Ancestral state reconstructions of (a) vein density (VD), (b) minimum spanning tree ratio (MST), and (c) loop circularity ratio (CR) at two scaled vein sizes (small, and medium). (d) Two metrics of venation architecture disparity, sum variances and median centroids. (e) abiotic proxies: global reconstruction of atmospheric average temperature (Temp.) (Scotese et al., 2021) and atmospheric carbon dioxide concentration (CO2) (Foster et al., 2017); and (f) biotic proxies: global insect diversification rates (Insect div. rates) (Condamine et al., 2016). Temporal trajectories for loop elongation rate and for large veins are not shown because they did not show significant evolutionary trends. In all panels, lines represent the median values averaged over ca. 10 Myr time-bins with standard deviation (panels a, b, c, f) or 95% confidence interval (panels d-e). Shaded vertical bars indicate the time of important geological events: L-D (Late Devonian mass-extinction); P-T (Permian-Triassic mass-extinction); T-J (Triassic-Jurassic mass-extinction); KTR (Cretaceous Terrestrial Revolution); K-P (Cretaceous-Paleogene mass-extinction).

References

1. Boyce, C. K., Brodribb, T. J., Feild, T. S. & Zwieniecki, M. A. Angiosperm leaf vein evolution was physiologically and environmentally transformative. *Proc. R. Soc. B Biol. Sci.* **276**, 1771–1776 (2009).
2. Sack, L. & Scoffoni, C. Leaf venation: structure, function, development, evolution, ecology and applications in the past, present and future. *New Phytol.* **198**, 983–1000 (2013).
3. Blonder, B. *et al.* Linking functional traits to multiscale statistics of leaf venation networks. *New Phytol.* **228**, 1796–1810 (2020).
4. Matos, I. S. *et al.* Leaf venation network architecture coordinates functional trade-offs across vein spatial scales: evidence for multiple alternative designs. *New Phytol.* nph.20037 (2024) doi:10.1111/nph.20037.

5. Bres, J., Sepulchre, P., Viovy, N. & Vuichard, N. The Cretaceous physiological adaptation of angiosperms to a declining pCO₂: a trait-oriented modelling approach. Preprint at https://doi.org/10.5194/bg-2021-139 (2021).
6. Beerling, D. J. Leaf Evolution: Gases, Genes and Geochemistry. *Ann. Bot.* **96**, 345–352 (2005).
7. Brodribb, T. J. & Feild, T. S. Leaf hydraulic evolution led a surge in leaf photosynthetic capacity during early angiosperm diversification. *Ecol. Lett.* **13**, 175–183 (2010).
8. Feild, T. S. *et al.* Fossil evidence for Cretaceous escalation in angiosperm leaf vein evolution. *Proc. Natl. Acad. Sci.* **108**, 8363–8366 (2011).
9. Boyce, C. K. & Knoll, A. H. Evolution of developmental potential and the multiple independent origins of leaves in Paleozoic vascular plants. *Paleobiology* **28**, 70–100 (2002).
10. Boyce, C. K. Patterns of segregation and convergence in the evolution of fern and seed plant leaf morphologies. *Paleobiology* **31**, 117–140 (2005).
11. Walls, R. L. Angiosperm leaf vein patterns are linked to leaf functions in a global-scale data set. *Am. J. Bot.* **98**, 244–253 (2011).
12. Kawai, K. & Okada, N. Roles of major and minor vein in leaf water deficit tolerance and structural properties in 11 temperate deciduous woody species. *Trees* **32**, 1573–1582 (2018).
13. Kawai, K. & Okada, N. How are leaf mechanical properties and water-use traits coordinated by vein traits? A case study in F agaceae. *Funct. Ecol.* **30**, 527–536 (2016).
14. Katifori, E., Szöllősi, G. J. & Magnasco, M. O. Damage and Fluctuations Induce Loops in Optimal Transport Networks. *Phys. Rev. Lett.* **104**, 048704 (2010).
15. Benton, M. J., Wilf, P. & Sauquet, H. The Angiosperm Terrestrial Revolution and the origins of modern biodiversity. *New Phytol.* **233**, 2017–2035 (2022).

16. Castiglione, S. *et al.* A new method for testing evolutionary rate variation and shifts in phenotypic evolution. *Methods Ecol. Evol.* **9**, 974–983 (2018).

17. Scotese, C. R., Song, H., Mills, B. J. W. & Van Der Meer, D. G. Phanerozoic paleotemperatures: The earth's changing climate during the last 540 million years. *Earth-Sci. Rev.* **215**, 103503 (2021).

18. Foster, G. L., Royer, D. L. & Lunt, D. J. Future climate forcing potentially without precedent in the last 420 million years. *Nat. Commun.* **8**, 14845 (2017).

19. Condamine, F. L., Clapham, M. E. & Kergoat, G. J. Global patterns of insect diversification: towards a reconciliation of fossil and molecular evidence? *Sci. Rep.* **6**, 19208 (2016).

20. Castiglione, S., Serio, C., Mondanaro, A., Melchionna, M. & Raia, P. Fast production of large, time-calibrated, informal supertrees with tree.merger. *Palaeontology* **65**, e12588 (2022).

21. Sack, L. *et al.* Developmentally based scaling of leaf venation architecture explains global ecological patterns. *Nat. Commun.* **3**, 837 (2012).

22. De Boer, H. J., Eppinga, M. B., Wassen, M. J. & Dekker, S. C. A critical transition in leaf evolution facilitated the Cretaceous angiosperm revolution. *Nat. Commun.* **3**, 1221 (2012).

23. Brodribb, T. J., Feild, T. S. & Sack, L. Viewing leaf structure and evolution from a hydraulic perspective. *Funct. Plant Biol.* **37**, 488 (2010).

24. Blonder, B., Violle, C., Bentley, L. P. & Enquist, B. J. Venation networks and the origin of the leaf economics spectrum. *Ecol. Lett.* **14**, 91–100 (2011).

25. Silvestro, D., Cascales-Miñana, B., Bacon, C. D. & Antonelli, A. Revisiting the origin and diversification of vascular plants through a comprehensive Bayesian analysis of the fossil record. *New Phytol.* **207**, 425–436 (2015).

931 26. Katifori, E. & Magnasco, M. O. Quantifying Loopy Network Architectures. *PLoS ONE*
932 **7**, e37994 (2012).
933 27. Brodribb, T. J., Feild, T. S. & Jordan, G. J. Leaf Maximum Photosynthetic Rate and
934 Venation Are Linked by Hydraulics. *Plant Physiol.* **144**, 1890–1898 (2007).
935 28. Niklas, K. J. Morphological evolution through complex domains of fitness. *Proc. Natl.*
936 *Acad. Sci.* **91**, 6772–6779 (1994).
937 29. Boyce, C. K. & Leslie, A. B. The Paleontological Context of Angiosperm Vegetative
938 Evolution. *Int. J. Plant Sci.* **173**, 561–568 (2012).
939 30. Ramírez-Barahona, S., Sauquet, H. & Magallón, S. The delayed and geographically
940 heterogeneous diversification of flowering plant families. *Nat. Ecol. Evol.* **4**, 1232–1238
941 (2020).
942 31. Blonder, B., Royer, D. L., Johnson, K. R., Miller, I. & Enquist, B. J. Plant Ecological
943 Strategies Shift Across the Cretaceous–Paleogene Boundary. *PLoS Biol.* **12**, e1001949 (2014).
944 32. Sperry, J. S., Hacke, U. G., Feild, T. S., Sano, Y. & Sikkema, E. H. Hydraulic
945 Consequences of Vessel Evolution in Angiosperms. *Int. J. Plant Sci.* **168**, 1127–1139 (2007).
946 33. Feild, T. S. & Wilson, J. P. Evolutionary Voyage of Angiosperm Vessel Structure-
947 Function and Its Significance for Early Angiosperm Success. *Int. J. Plant Sci.* **173**, 596–609
948 (2012).
949 34. Ueno, O., Kawano, Y., Wakayama, M. & Takeda, T. Leaf Vascular Systems in C3 and
950 C4 Grasses: A Two-dimensional Analysis. *Ann. Bot.* **97**, 611–621 (2006).
951 35. Hughes, M., Gerber, S. & Wills, M. A. Clades reach highest morphological disparity
952 early in their evolution. *Proc. Natl. Acad. Sci.* **110**, 13875–13879 (2013).
953 36. Oyston, J. W., Hughes, M., Gerber, S. & Wills, M. A. Why should we investigate the

morphological disparity of plant clades? *Ann. Bot.* **117**, 859–879 (2016).

37. Beerling, D. J. & Berner, R. A. Feedbacks and the coevolution of plants and atmospheric CO 2. *Proc. Natl. Acad. Sci.* **102**, 1302–1305 (2005).

38. Labandeira, C. C. & Currano, E. D. The Fossil Record of Plant-Insect Dynamics. *Annu. Rev. Earth Planet. Sci.* **41**, 287–311 (2013).

39. Coley, P. D. & Barone, J. A. HERBIVORY AND PLANT DEFENSES IN TROPICAL FORESTS. *Annu. Rev. Ecol. Syst.* **27**, 305–335 (1996).

40. Wiens, J. J., Lapoint, R. T. & Whiteman, N. K. Herbivory increases diversification across insect clades. *Nat. Commun.* **6**, 8370 (2015).

41. Rashid War, A. *et al.* Plant Defense Against Herbivory and Insect Adaptations. *AoB PLANTS* (2018) doi:10.1093/aobpla/ply037.

42. Wilf, P. *et al.* An image dataset of cleared, x-rayed, and fossil leaves vetted to plant family for human and machine learning. *PhytoKeys* **187**, 93–128 (2021).

43. Matos, I. S. *et al.* Leaf architecture and functional traits for 122 species at the University of California Botanical Garden at Berkeley. *Ecology* **105**, e4436 (2024).

44. Niewiadomski, I., *et al.* A comprehensive illustrated protocol for clearing, mounting, and imaging leaf venation networks. *Appl. Plant Sci.* **e70002** (2025).

45. Deng, S.-H. *et al.* Plant fossils from the Lower Jurassic coal-bearing formation of central Inner Mongolia of China and their implications for palaeoclimate. *Palaeoworld* **26**, 279–316 (2017).

46. Escapa, I. H., Bomfleur, B., Cuneo, N. R. & Scasso, R. A new marattiaceous fern from the Lower Jurassic of Patagonia (Argentina): the renaissance of *Marattiopsis*. *J. Syst. Palaeontol.* **13**, 677–689 (2015).

47. McLoughlin, S. & Pott, C. The Jurassic flora of Western Australia. *GFF* **131**, 113–136

(2009).

48. Pott, C. & McLoughlin, S. Bennettitalean foliage in the Rhaetian–Bajocian (latest Triassic–Middle Jurassic) floras of Scania, southern Sweden. *Rev. Palaeobot. Palynol.* **158**, 117–166 (2009).

49. Na, Y. *et al.* A brief introduction to the Middle Jurassic Daohugou Flora from Inner Mongolia, China. *Rev. Palaeobot. Palynol.* **247**, 53–67 (2017).

50. Pott, C. & Jiang, B. Plant remains from the Middle–Late Jurassic Daohugou site of the Yanliao Biota in Inner Mongolia, China. *Acta Palaeobot.* **57**, 185–222 (2017).

51. Scanu, G. G., Kustatscher, E. & Pittau, P. The Jurassic plant fossils of the Lovisato Collection: preliminary notes. *Boll. Della Soc. Paleontol. Ital.* 71–84 (2012) doi:10.4435/BSPI.2012.9.

52. McElwain, J. C., Yiotis, C. & Lawson, T. Using modern plant trait relationships between observed and theoretical maximum stomatal conductance and vein density to examine patterns of plant macroevolution. *New Phytol.* **209**, 94–103 (2016).

53. Zhang, J. & Qian, H. U.Taxonstand: An R package for standardizing scientific names of plants and animals. *Plant Divers.* **45**, 1–5 (2023).

54. The Angiosperm Phylogeny Group. An update of the Angiosperm Phylogeny Group classification for the orders and families of flowering plants: APG IV. *Bot. J. Linn. Soc.* **181**, 1–20 (2016).

55. Jin, Y. & Qian, H. V.PhyloMaker2: An updated and enlarged R package that can generate very large phylogenies for vascular plants. *Plant Divers.* **44**, 335–339 (2022).

56. Kumar, S., Stecher, G., Suleski, M. & Hedges, S. B. TimeTree: A Resource for Timelines, Timetrees, and Divergence Times. *Mol. Biol. Evol.* **34**, 1812–1819 (2017).

1001 57. Cleal, C. J. & Shute, C. H. The systematic and palaeoecological value of foliage anatomy
1002 in Late Palaeozoic medullosalean seed-plants. *J. Syst. Palaeontol.* **10**, 765–800 (2012).
1003 58. Serio, C. *et al.* Macroevolution of Toothed Whales Exceptional Relative Brain Size. *Evol.*
1004 *Biol.* **46**, 332–342 (2019).
1005 59. Xu, H., Blonder, B., Jodra, M., Malhi, Y. & Fricker, M. Automated and accurate
1006 segmentation of leaf venation networks via deep learning. *New Phytol.* **229**, 631–648 (2021).
1007 60. Blonder, B. *et al.* Structural and defensive roles of angiosperm leaf venation network
1008 reticulation across an Andes–Amazon elevation gradient. *J. Ecol.* **106**, 1683–1699 (2018).
1009 61. Castiglione, S. *et al.* Simultaneous detection of macroevolutionary patterns in phenotypic
1010 means and rate of change with and within phylogenetic trees including extinct species. *PLOS*
1011 *ONE* **14**, e0210101 (2019).
1012 62. Zuntini, A. R. *et al.* Phylogenomics and the rise of the angiosperms. *Nature* **629**, 843–850
1013 (2024).
1014 63. Benjamini, Y. & Hochberg, Y. Controlling the False Discovery Rate: A Practical and
1015 Powerful Approach to Multiple Testing. *J. R. Stat. Soc. Ser. B Stat. Methodol.* **57**, 289–300
1016 (1995).
1017 64. Guillerme, T. dispRity: A modular R package for measuring disparity. *Methods Ecol.*
1018 *Evol.* **9**, 1755–1763 (2018).
1019 65. Guillerme, T. & Cooper, N. Time for a rethink: time sub-sampling methods in disparity-
1020 through-time analyses. *Palaeontology* **61**, 481–493 (2018).
1021 66. Matos, I. S., Bradley, V., Mann, J., Xie, E., Madhavan, S., Sharma, S, Niewiadomski, I.,
1022 Echevarria, A., Tomaka, C., Carlos, S., Antonio, M., Chu, A., Scudder, M., Yokota, N., Park, H.,
1023 Vuong, N., Boakye, M., Duarte, M. A., Pechuzal, C., Aparecido, L. M., Guevara Heredia, E.,
1024 Cardenas, R., Enquist, B. J., Erwin, D. M., Forbes, H., Dexter, K., Fricker, M., & Blonder, B.,

Macroevolutionary trends in leaf venation network architecture, Zenodo, https://doi.org/10.5281/zenodo.13300782, 2025.

67. Matos, I., Boakye, M., Antonio, M., Carlos, S., Chu, A., Duarte, M. A., Echevarria, A., Fontao, A., Garcia, L., Huang, L., Carrillo Johnson, B., Joshi, S., Kalantar, D., Madhavan, S., McDonough, S., Niewiadomski, I., Nguyen, N., Park, H. J., Pechuzal, C., Rohde, J., Sahu, R., Scudder, M., Sharma, S., Sneor, L., To, J., Vu, B., Vuong, N., Yokota, N., Aparecido, L. M., Forbes, H., Fricker, M., & Blonder, B., Leaf architecture and functional traits for 122 species at the University of California at Berkeley botanical garden, Dryad, https://doi.org/10.5061/dryad.1g1jwsv36, 2024.

68. Boakye, M., Adu-Bredu, S., Duah-Gyamfi, A., Djagbletey, G., Manu, E. A., Antonio, M., Carlos, S., Echevarria, A., Matos, I. S., Niewiadomski, I., Vu, B., Fricker, M., & Blonder, B. W., Leaf venation network architectural traits along a forest-savannah gradient in Ghana, Zenodo,https://doi.org/10.5281/zenodo.15217651, 2025.

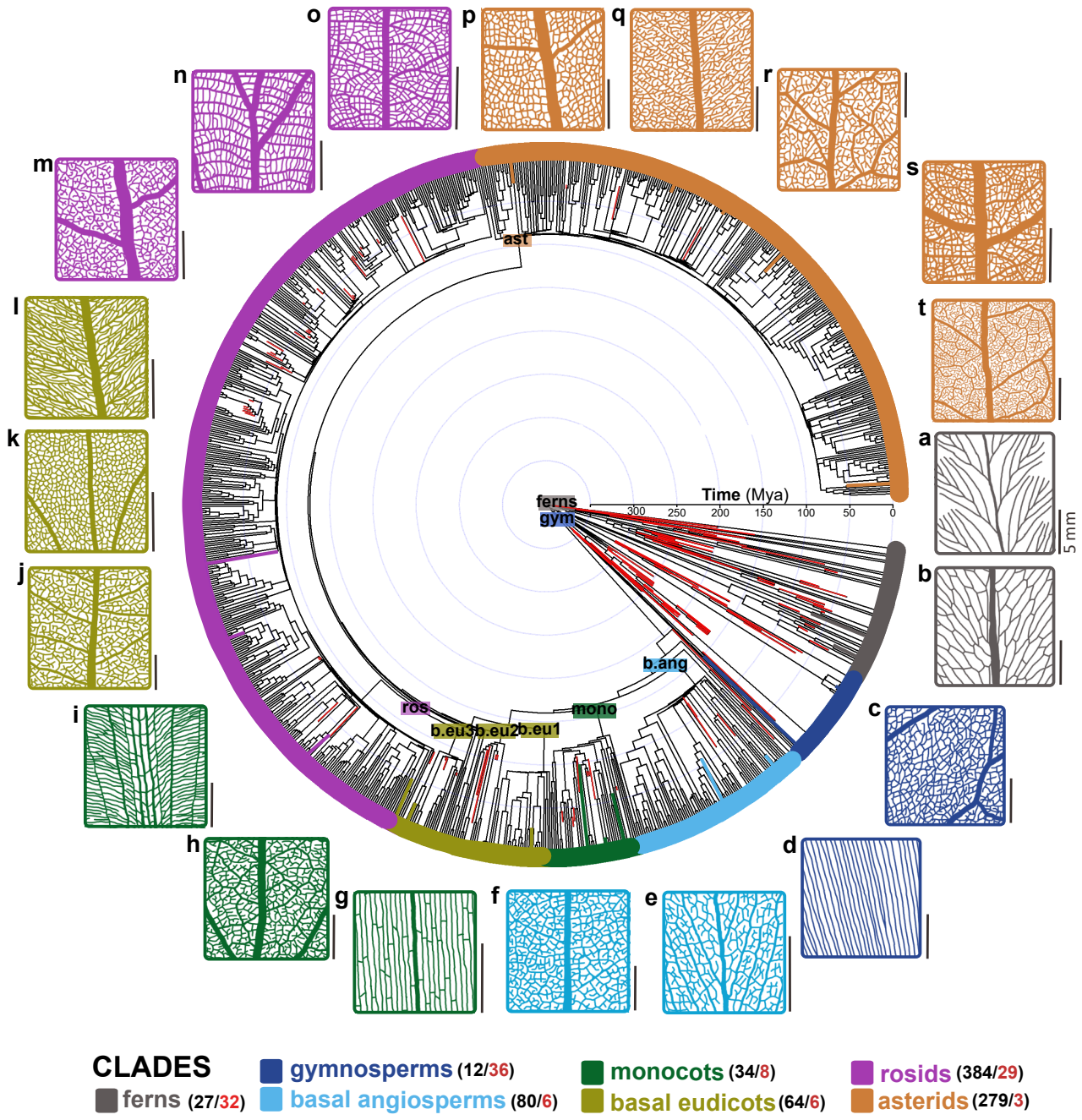
o
p
q
n
r
m
s
l
t
k
a
j
b
i
c
h
d
g
f
e
ast
ferns
gym
Time (Mya)
300
250
200
150
100
50
0
5 mm
b.ang
ros
mono
b.eu3
b.eu2
b.eu1
CLADES
ferns (27/32)
gymnosperms (12/36)
basal angiosperms (80/6)
monocots (34/8)
basal eudicots (64/6)
rosids (384/29)
asterids (279/3)

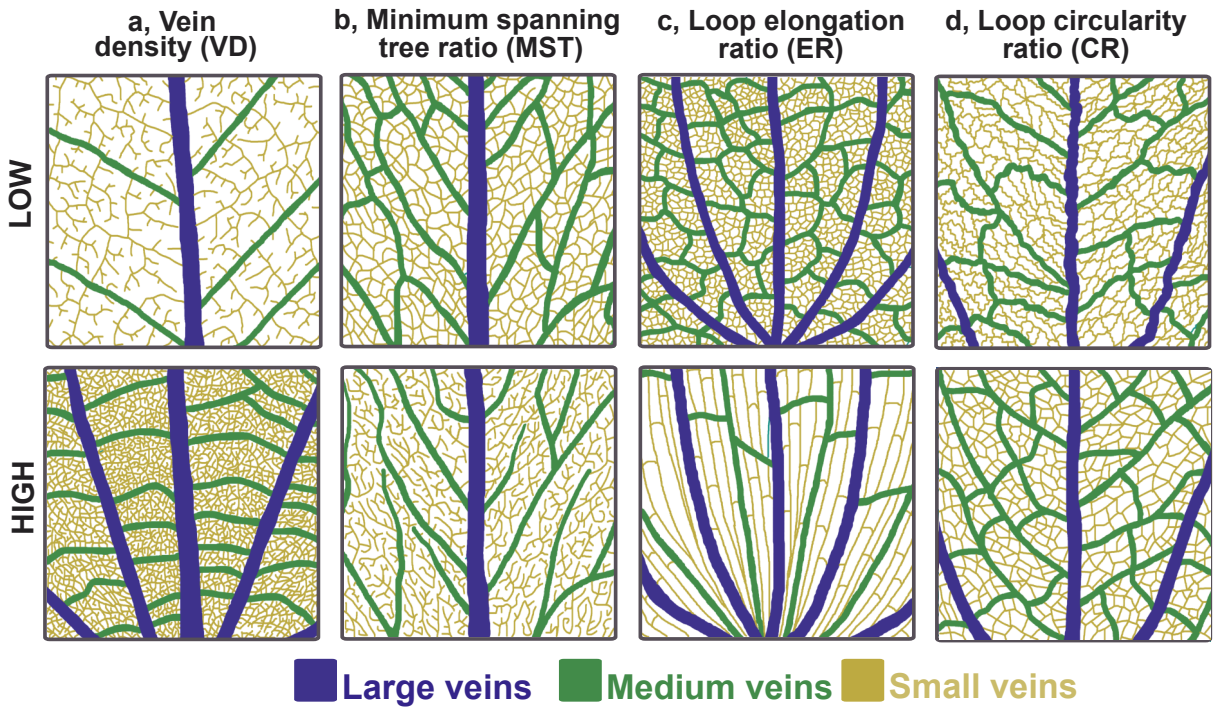
a, Vein density (VD)
b, Minimum spanning tree ratio (MST)
c, Loop elongation ratio (ER)
d, Loop circularity ratio (CR)
LOW
HIGH
Large veins
Medium veins
Small veins

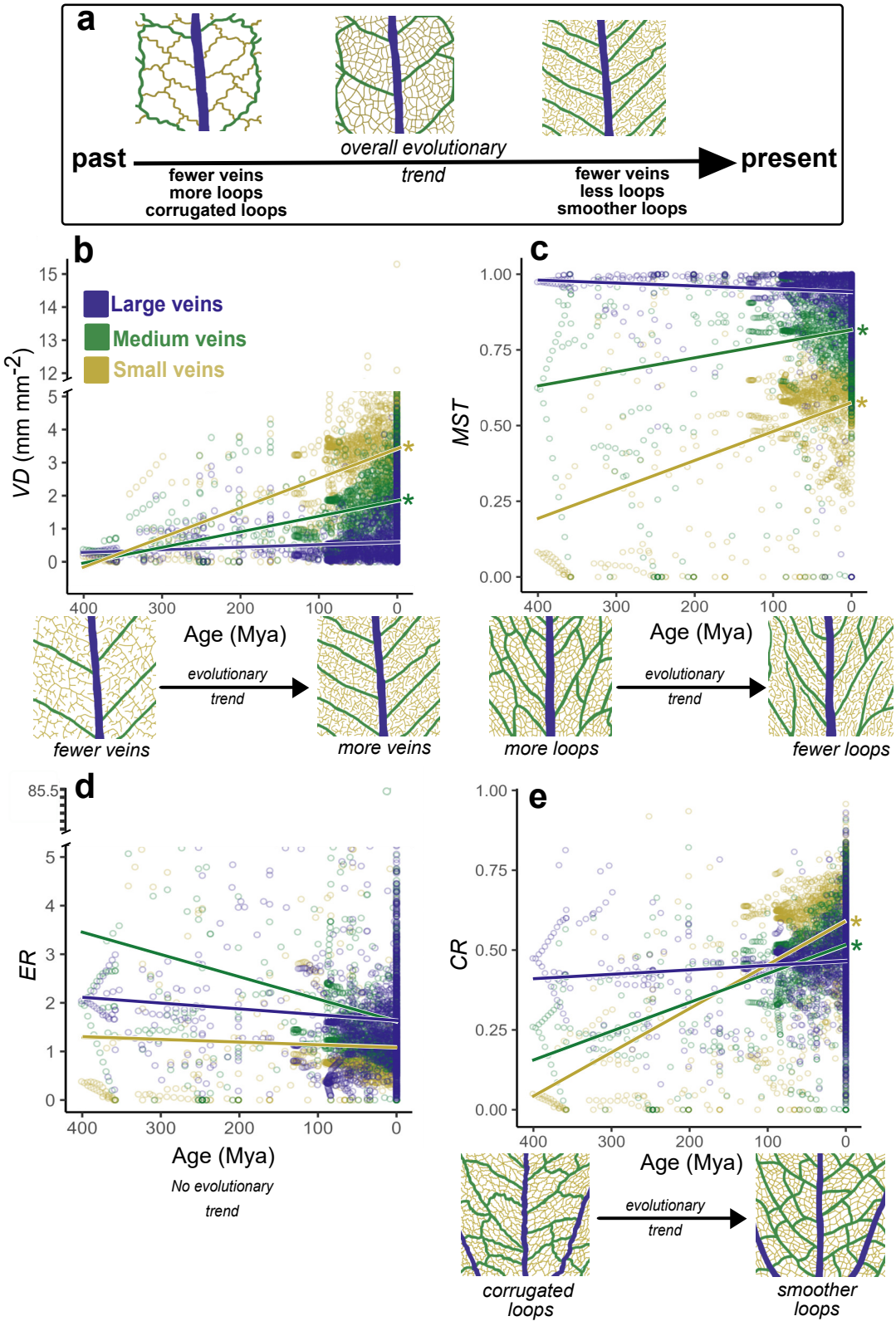
a
past
present
overall evolutionary trend
fewer veins
more loops
corrugated loops
fewer veins
less loops
smoother loops
b
Large veins
Medium veins
Small veins
VD (mm mm-2)
Age (Mya)
evolutionary trend
fewer veins
more veins
c
MST
Age (Mya)
evolutionary trend
more loops
fewer loops
d
ER
Age (Mya)
No evolutionary trend
e
CR
Age (Mya)
evolutionary trend
corrugated loops
smoother loops

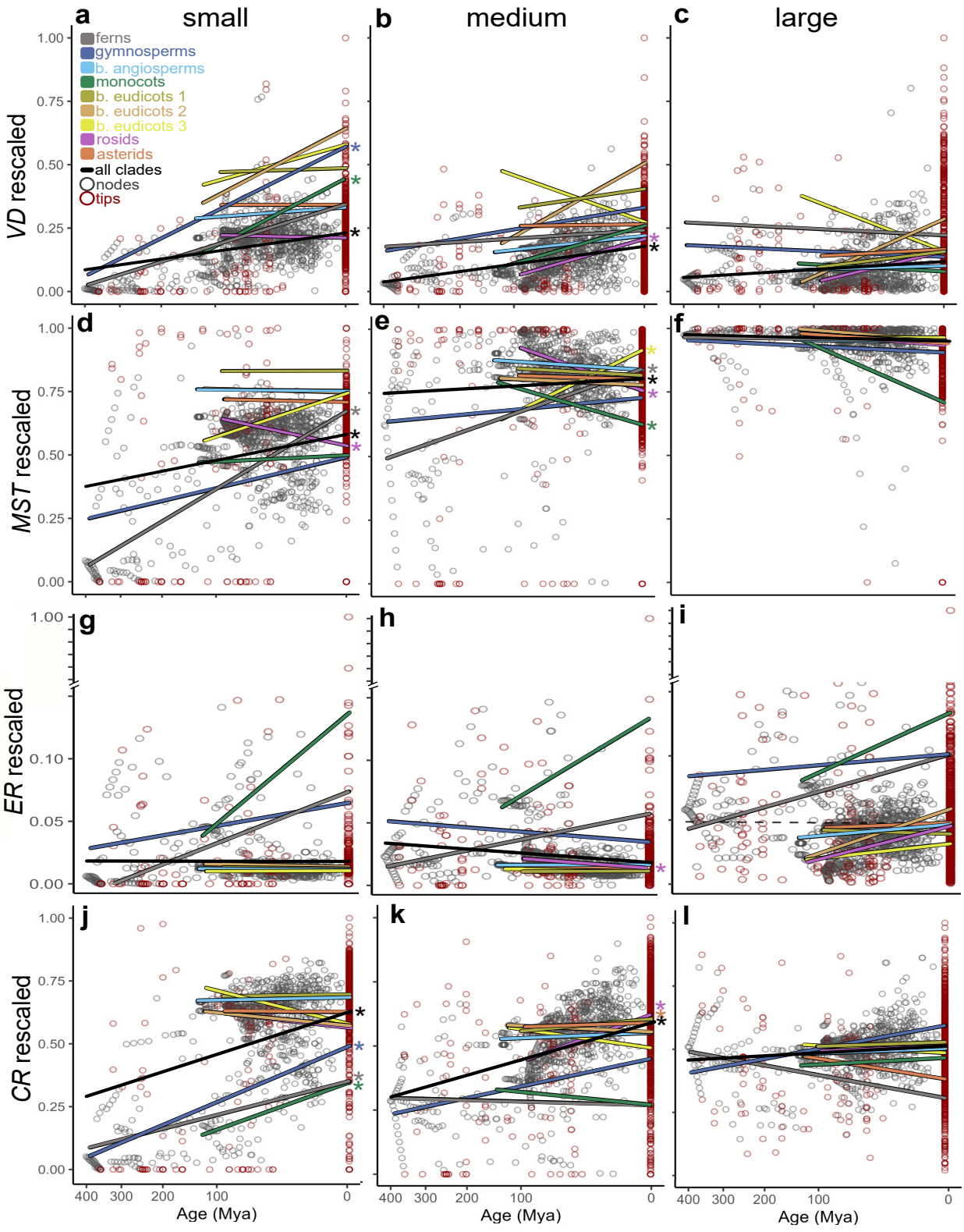
a
small
b
medium
c
large
ferns
gymnosperms
b. angiosperms
monocots
b. eudicots 1
b. eudicots 2
b. eudicots 3
rosids
asterids
all clades
nodes
tips
VD rescaled
MST rescaled
ER rescaled
CR rescaled
d
e
f
g
h
i
j
k
l
1.00
0.75
0.50
0.25
0.00
0.10
0.05
400
300
200
100
0
Age (Mya)

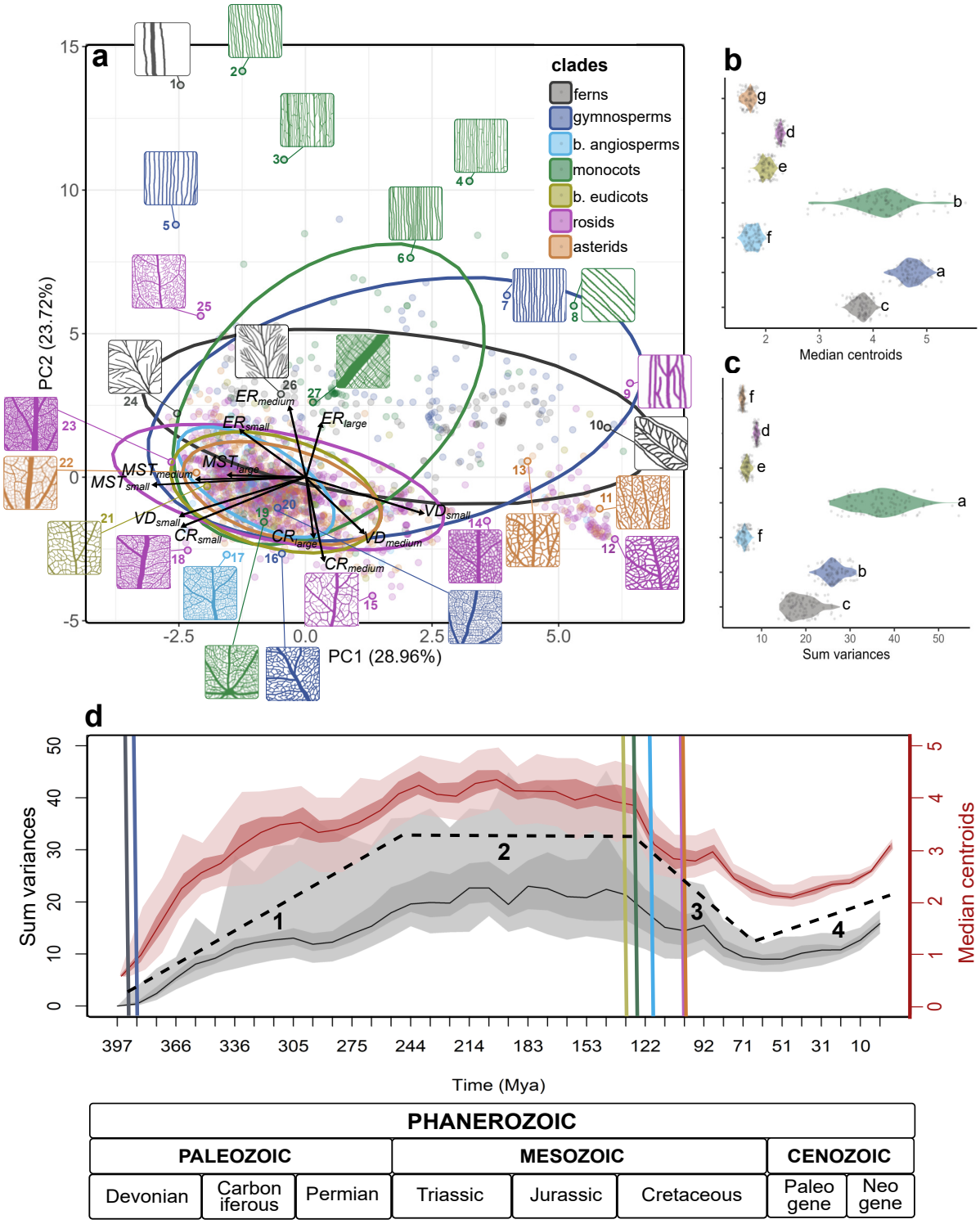
a
clades
ferns
gymnosperms
b. angiosperms
monocots
b. eudicots
rosids
asterids
PC2 (23.72%)
PC1 (28.96%)
ER_medium
ER_small
ER_large
MST_medium
MST_small
MST_large
VD_small
VD_medium
CR_small
CR_large
CR_medium
b
Median centroids
c
Sum variances
d
Sum variances
Median centroids
Time (Mya)
1
2
3
4
PHANEROZOIC
PALEOZOIC
MESOZOIC
CENOZOIC
Devonian
Carbon iferous
Permian
Triassic
Jurassic
Cretaceous
Paleo gene
Neo gene

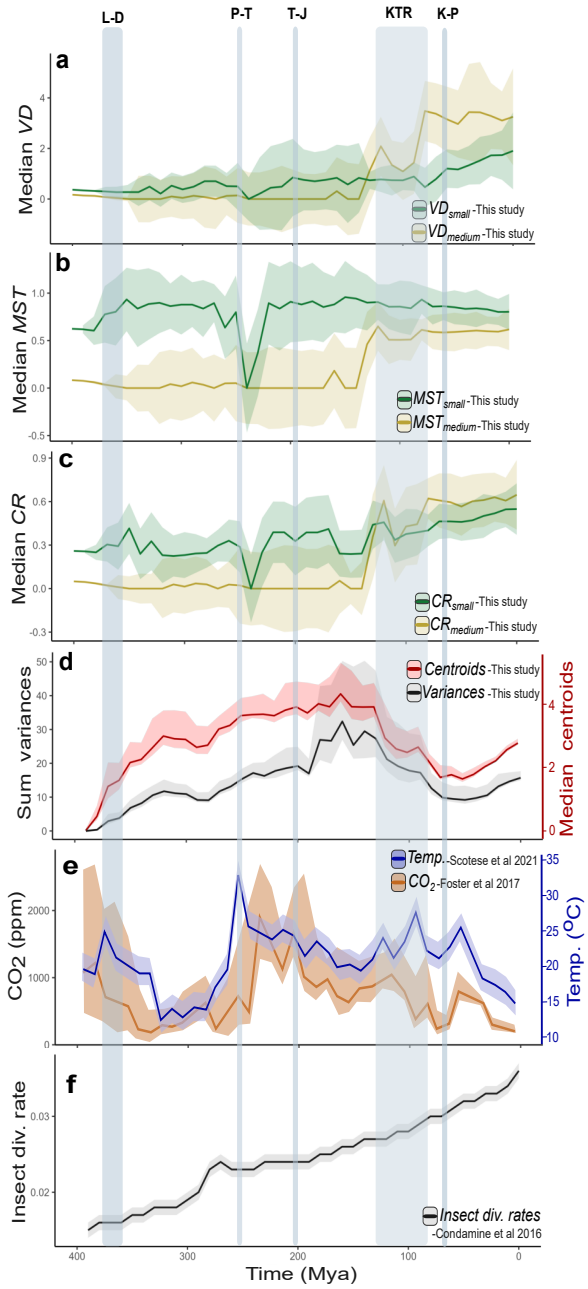
L-D
P-T
T-J
KTR
K-P
a
Median VD
VDsmall-This study
VDmedium-This study
b
Median MST
MSTsmall-This study
MSTmedium-This study
c
Median CR
CRsmall-This study
CRmedium-This study
d
Sum variances
Median centroids
Centroids-This study
Variances-This study
e
CO2 (ppm)
Temp. (°C)
Temp.-Scotese et al 2021
CO2-Foster et al 2017
f
Insect div. rate
Insect div. rates
-Condamine et al 2016
Time (Mya)
PHANEROZOIC
PALEOZOIC
MESOZOIC
CENOZOIC
Devonian
Carboniferous
Permian
Triassic
Jurassic
Cretaceous
Paleogene
Neo gene

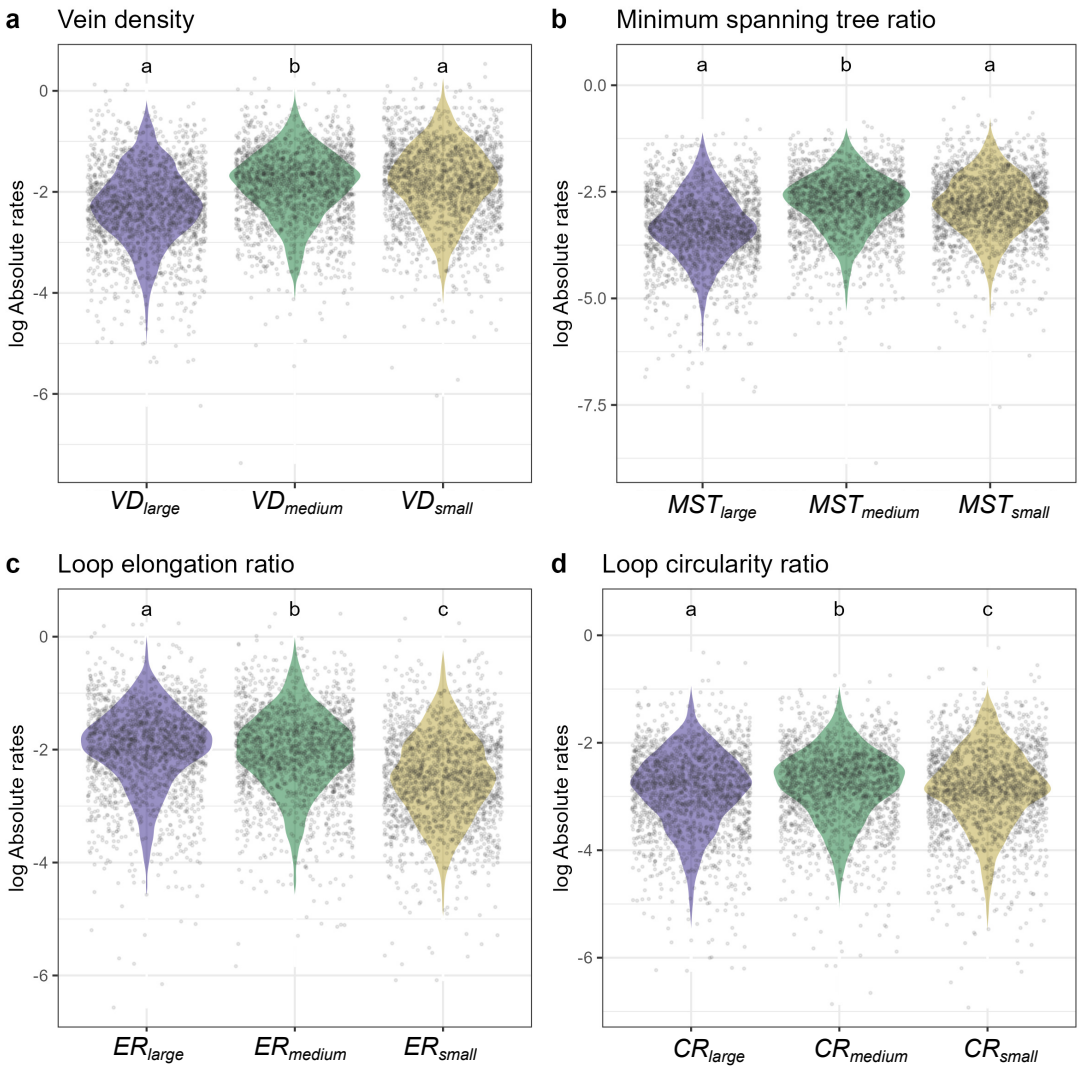
a
Vein density
log Absolute rates
0
-2
-4
-6
a
b
a
VD large
VD medium
VD small
b
Minimum spanning tree ratio
log Absolute rates
0.0
-2.5
-5.0
-7.5
a
b
a
MST large
MST medium
MST small
c
Loop elongation ratio
log Absolute rates
0
-2
-4
-6
a
b
c
ER large
ER medium
ER small
d
Loop circularity ratio
log Absolute rates
0
-2
-4
-6
a
b
c
CR large
CR medium
CR small

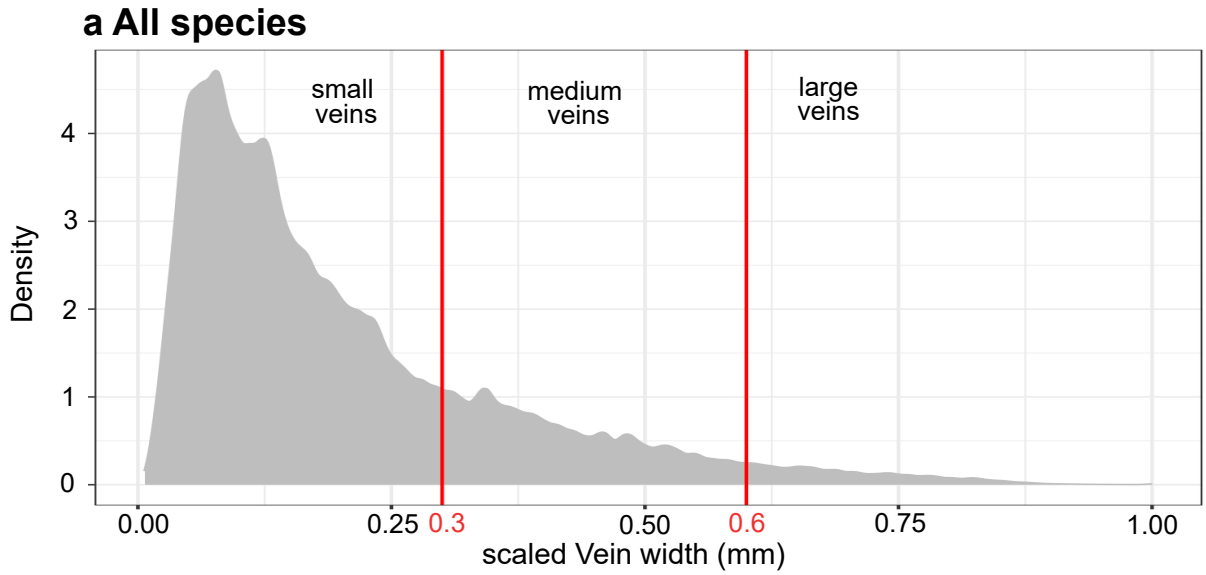
a All species
small veins
medium veins
large veins
Density
0
1
2
3
4
0.00
0.25
0.3
0.50
0.6
0.75
1.00
scaled Vein width (mm)

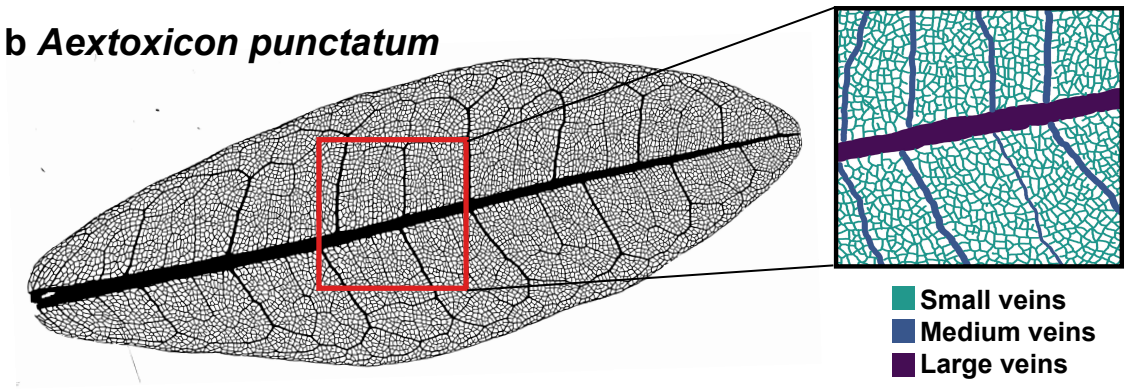
b Aextoxicon punctatum
Small veins
Medium veins
Large veins

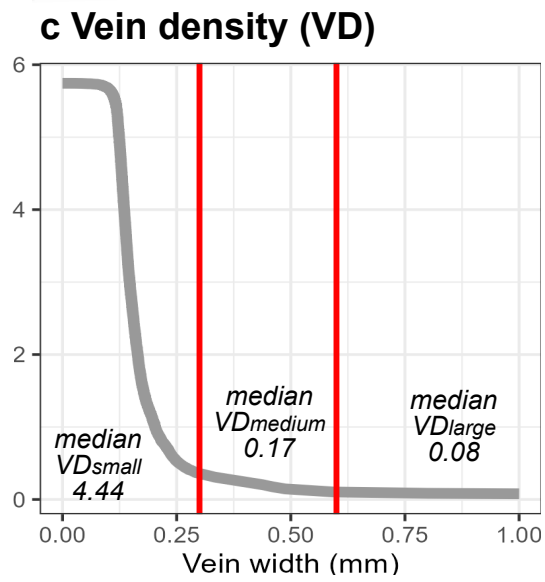
c Vein density (VD)
median VDsmall 4.44
median VDmedium 0.17
median VDlarge 0.08
0
2
4
6
0.00
0.25
0.50
0.75
1.00
Vein width (mm)

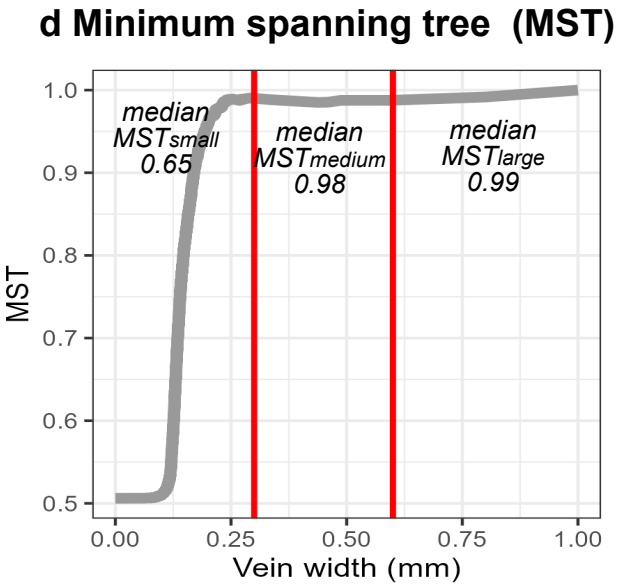
d Minimum spanning tree (MST)
median MSTsmall 0.65
median MSTmedium 0.98
median MSTlarge 0.99
MST
0.5
0.6
0.7
0.8
0.9
1.0
0.00
0.25
0.50
0.75
1.00
Vein width (mm)

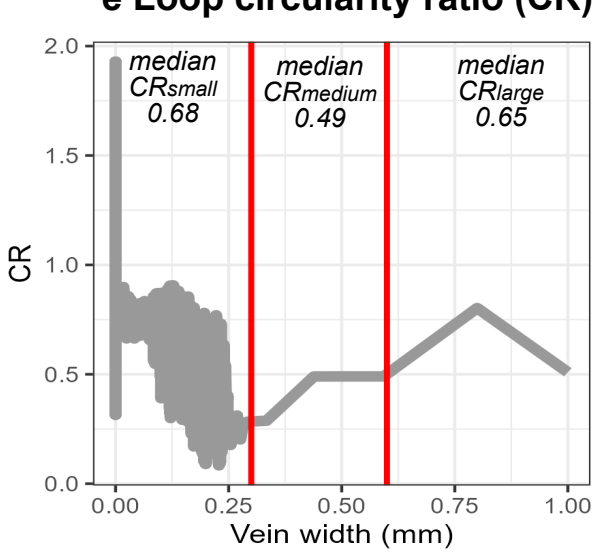
e Loop circularity ratio (CR)
median CRsmall 0.68
median CRmedium 0.49
median CRlarge 0.65
CR
0.0
0.5
1.0
1.5
2.0
0.00
0.25
0.50
0.75
1.00
Vein width (mm)

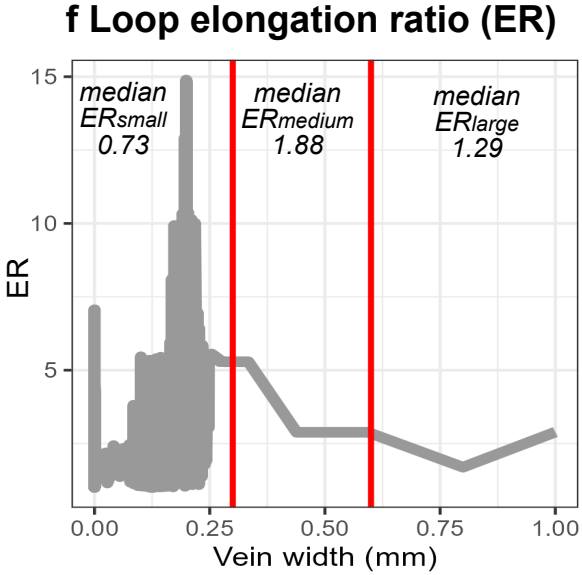
f Loop elongation ratio (ER)
median ERsmall 0.73
median ERmedium 1.88
median ERlarge 1.29
ER
5
10
15
0.00
0.25
0.50
0.75
1.00
Vein width (mm)

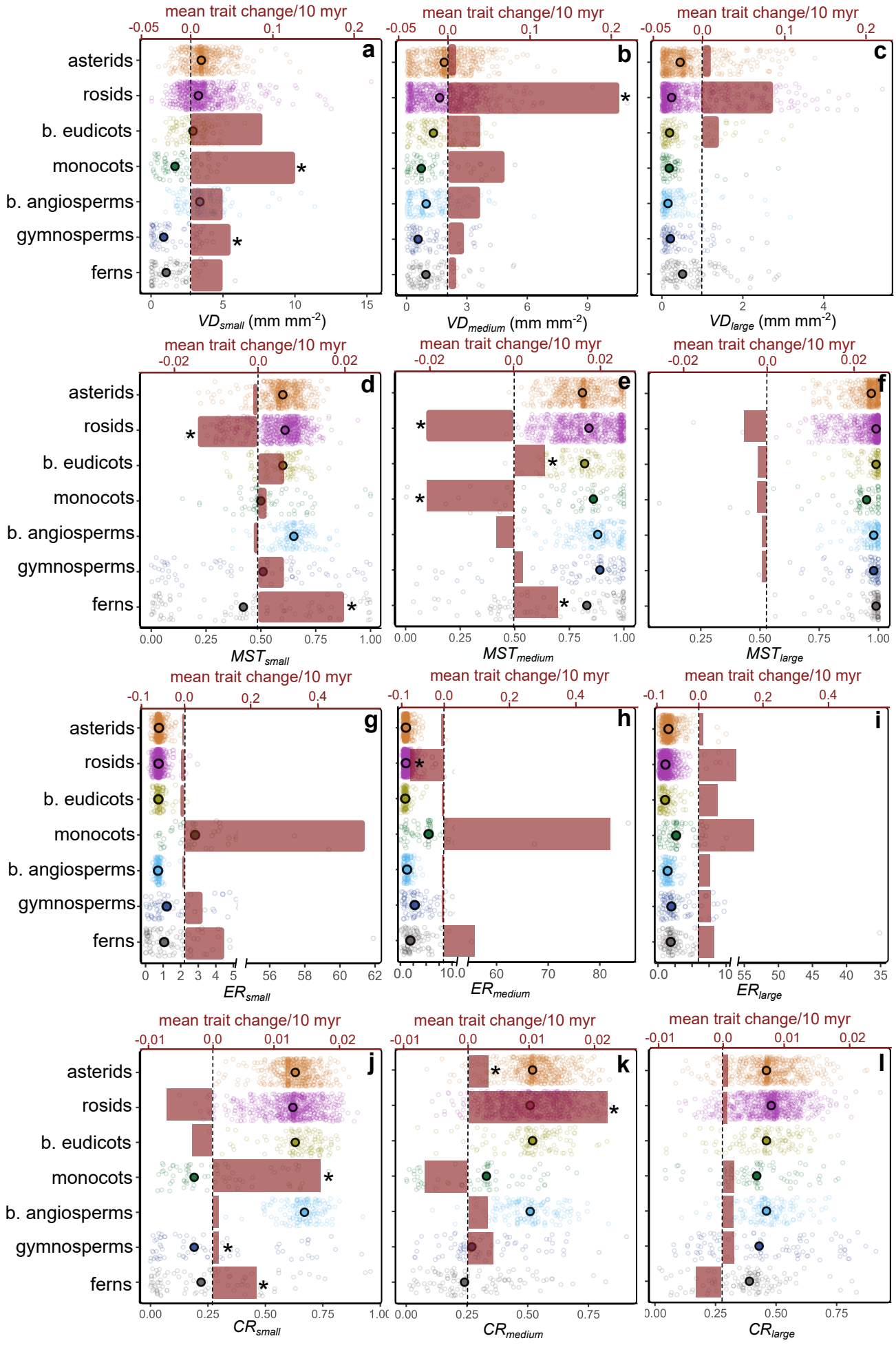
mean trait change/10 myr
asterids
rosids
b. eudicots
monocots
b. angiosperms
gymnosperms
ferns
a
b
c
d
e
f
g
h
i
j
k
l
VD_{small} (mm mm^{-2})
VD_{medium} (mm mm^{-2})
VD_{large} (mm mm^{-2})
MST_{small}
MST_{medium}
MST_{large}
ER_{small}
ER_{medium}
ER_{large}
CR_{small}
CR_{medium}
CR_{large}

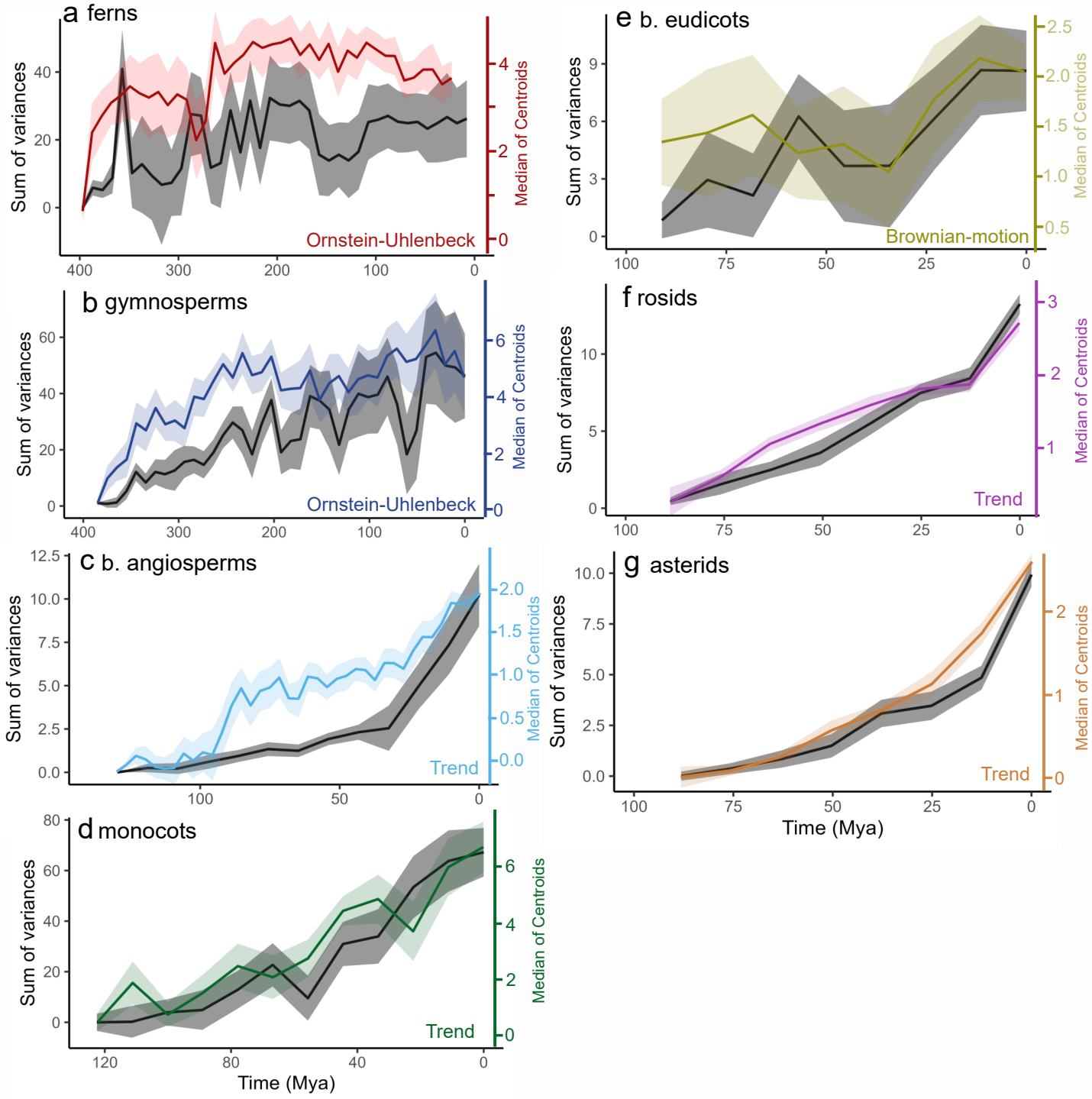
a ferns
Sum of variances
Median of Centroids
Ornstein-Uhlenbeck
b gymnosperms
Sum of variances
Median of Centroids
Ornstein-Uhlenbeck
c b. angiosperms
Sum of variances
Median of Centroids
Trend
d monocots
Sum of variances
Median of Centroids
Trend
Time (Mya)
e b. eudicots
Sum of variances
Median of Centroids
Brownian-motion
f rosids
Sum of variances
Median of Centroids
Trend
g asterids
Sum of variances
Median of Centroids
Trend
Time (Mya)

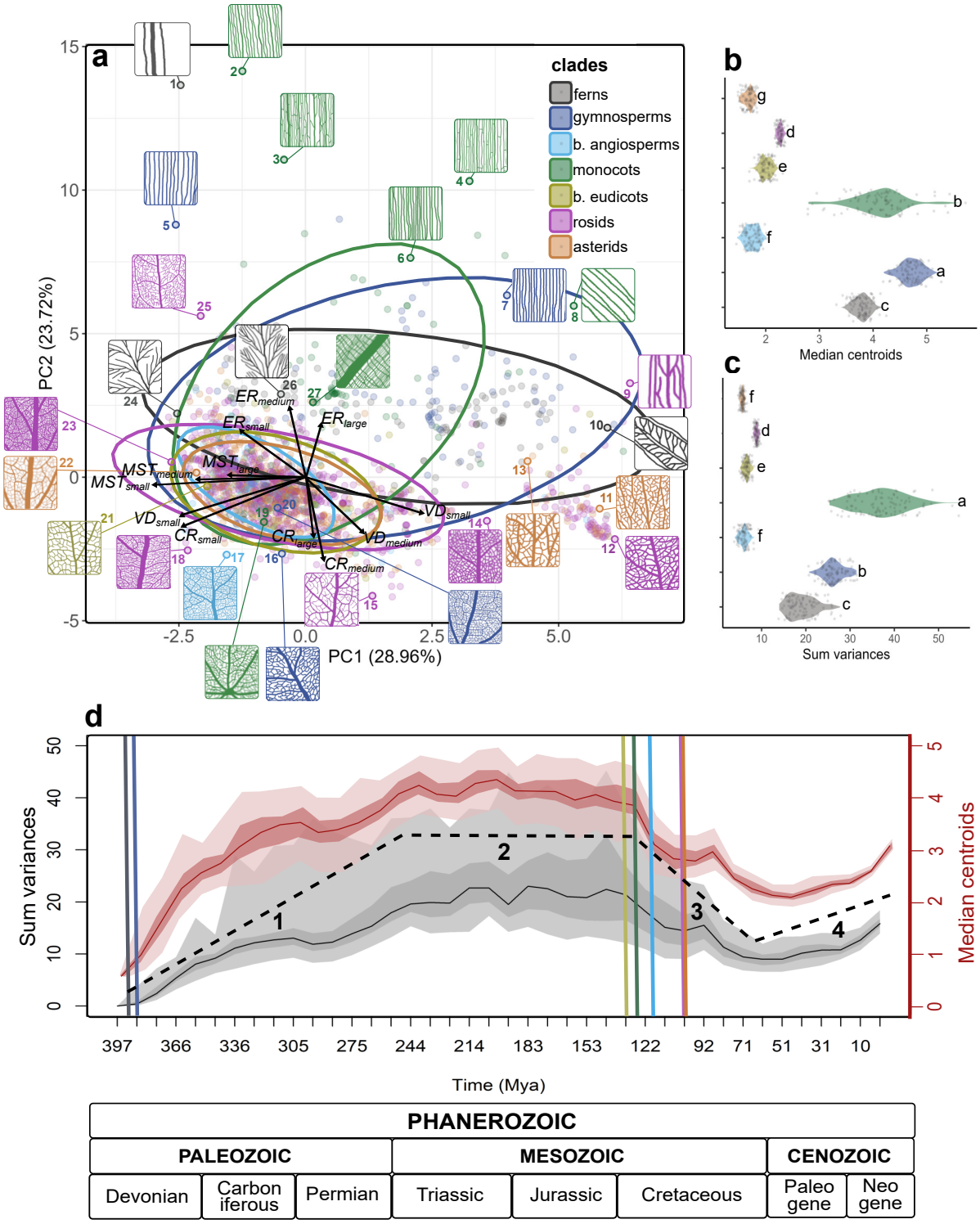
a
clades
ferns
gymnosperms
b. angiosperms
monocots
b. eudicots
rosids
asterids
PC2 (23.72%)
PC1 (28.96%)
ER_medium
ER_small
ER_large
MST_medium
MST_small
MST_large
VD_small
VD_medium
CR_small
CR_large
CR_medium
b
Median centroids
c
Sum variances
d
Sum variances
Median centroids
Time (Mya)
1
2
3
4
PHANEROZOIC
PALEOZOIC
MESOZOIC
CENOZOIC
Devonian
Carbon iferous
Permian
Triassic
Jurassic
Cretaceous
Paleo gene
Neo gene

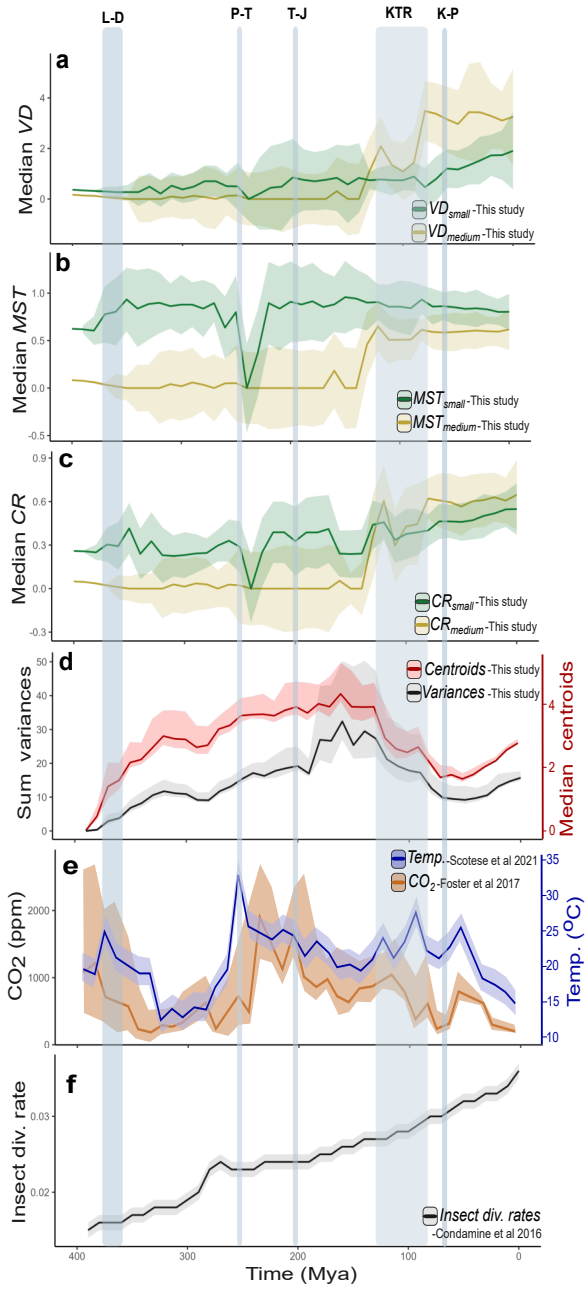
L-D
P-T
T-J
KTR
K-P
a
Median VD
VDsmall-This study
VDmedium-This study
b
Median MST
MSTsmall-This study
MSTmedium-This study
c
Median CR
CRsmall-This study
CRmedium-This study
d
Sum variances
Median centroids
Centroids-This study
Variances-This study
e
CO2 (ppm)
Temp. (°C)
Temp.-Scotese et al 2021
CO2-Foster et al 2017
f
Insect div. rate
Insect div. rates
-Condamine et al 2016
Time (Mya)
PHANEROZOIC
PALEOZOIC
MESOZOIC
CENOZOIC
Devonian
Carboniferous
Permian
Triassic
Jurassic
Cretaceous
Paleogene
Neo gene